



1N-37
392603

TECHNICAL NOTE

D-476

BONDED AND SEALED EXTERNAL INSULATIONS FOR LIQUID-
HYDROGEN-FUELED ROCKET TANKS DURING
ATMOSPHERIC FLIGHT

By V. H. Gray, T. F. Gelder, R. P. Cochran,
and J. H. Goodykoontz

Lewis Research Center
Cleveland, Ohio

NATIONAL AERONAUTICS AND SPACE ADMINISTRATION
WASHINGTON

October 1960

1

2

3

CONTENTS

	Page
SUMMARY	1
INTRODUCTION	1
APPARATUS AND PROCEDURE	3
Thermal-Conductivity Tests	3
Conductivity meter	3
Tank boiloff tests	4
Sealing Tests	5
High-Temperature Tests	5
RESULTS AND DISCUSSION	7
Thermal Conductivity	7
Self-supporting insulations	7
Filled-honeycomb insulations	8
Tank tests	8
Sealing	10
Strength of Bonded-On Insulations at Cryogenic Temperatures	10
High-Temperature Performance	11
Corkboard	11
Balsa	12
Faced honeycombs	12
INSULATION FOR A SPECIFIC VEHICLE	14
Ground Performance	14
Flight Performance	16
COMMENTS AND RECOMMENDATIONS	16
SUMMARY OF RESULTS	17
APPENDIXES	19
A - SYMBOLS	19
B - STRENGTH OF INSULATIONS AND BOND TO ALUMINUM AT CRYOGENIC TEMPERATURES, by Morgan P. Hanson	20
C - STEP METHOD OF APPROXIMATE NUMERICAL CALCULATION OF ONE- DIMENSIONAL TRANSIENT HEAT CONDUCTION WITH VARIABLE THERMAL PROPERTIES, by William Lewis	23
REFERENCES	27
TABLES	29
FIGURES	32

NATIONAL AERONAUTICS AND SPACE ADMINISTRATION

TECHNICAL NOTE D-476

BONDED AND SEALED EXTERNAL INSULATIONS FOR LIQUID-HYDROGEN-
FUELED ROCKET TANKS DURING ATMOSPHERIC FLIGHT

By V. H. Gray, T. F. Gelder, R. P. Cochran,
and J. H. Goodykoontz

SUMMARY

Several currently available nonmetallic insulation materials that may be bonded onto liquid-hydrogen tanks and sealed against air penetration into the insulation have been investigated for application to rockets and spacecraft. Experimental data were obtained on the thermal conductivities of various materials in the cryogenic temperature range, as well as on the structural integrity and ablation characteristics of these materials at high temperatures occasioned by aerodynamic heating during atmospheric escape. Of the materials tested, commercial corkboard has the best overall properties for the specific requirements imposed during atmospheric flight of a high-acceleration rocket vehicle.

INTRODUCTION

With the advent of liquid hydrogen as a fuel for rockets and spacecraft, the need for insulation on the tanks while on the ground and in atmospheric flight has arisen. Without insulation, air will continually condense on the metal tank walls, which will be colder than the condensation temperature of air because of the very low boiling temperature of hydrogen. In condensing, this air will release its heat of vaporization and thereby generate a rapid flow of heat into the hydrogen. Such heat flows will cause rapid boiling of the hydrogen, which will result in large fuel venting losses and/or tank pressure rises. To reduce these losses markedly, insulation is required to maintain the exposed surface temperatures at least above the condensation temperature of air. The type and amount of insulation depend entirely on the specific vehicle and flight program.

The problem of designing tank insulation for hydrogen-fueled rockets is complicated by several exacting and sometimes contradictory requirements of the materials. The insulation, for example, must be lightweight yet possess enough strength to withstand aerodynamic forces. It should

E-806

CP-1

be slightly flexible at cryogenic temperatures and yet retain enough stiffness at high temperatures caused by aerodynamic heating so that nothing worse than slow, orderly surface ablation will result. Also, the insulation should have and retain a low thermal conductivity, despite local temperatures below the air condensation temperature.

Very little specific information on this tank insulation problem is available in the literature; however, there are some general state-of-the-art publications, such as references 1 and 2. In addition, several papers contain helpful information about particular phases of the problem, such as references 3 to 6. Many of the problem areas, however, are nearly devoid of published data; notably, the thermal conductivities of insulations at mean temperatures as low as -320° F, the resistance of insulations to air penetration and liquefaction at temperatures below -320° F, and the ablation resistance of common insulations at elevated temperatures.

The objective of this investigation is to obtain engineering data in the previously mentioned problem areas for a variety of insulation materials to provide a basis for design of hydrogen tank insulations for atmospheric flight of forthcoming rockets. Following this, a particular rocket vehicle and flight plan will be considered merely as an example, for which the best overall insulation design will be composed from the available data.

In this study, emphasis is placed on the problems of insulating rocket vehicles having high velocities while in the atmosphere (high booster accelerations). These atmospheric velocities impose large aerodynamic loads and heat fluxes on the insulation. Consequently, insulation strength and resistance to high temperatures become important factors. These aerodynamic considerations greatly restrict the range of materials and designs that may be used. The present study is limited to the non-metallic insulations listed in table I. These insulations fall into two categories: (1) self-supporting types that may be bonded directly onto metal hydrogen tanks (aluminum herein), and (2) nonstructural types to be used as filler materials in the cells of bonded-on honeycomb sandwiches. Some current insulations were not tested herein: pressed-fiber sheets and unreinforced plastic foams (both have dubious strength at high velocity and temperature); also, ceramic and glass foams (stiff and difficult to fabricate in thin sections).

This investigation was conducted in research facilities of the NASA Lewis Research Center. Experimental tests of materials were made in four main categories: thermal conductivity, sealability, strength, and high-temperature resistance. Temperature effects were investigated over a range from -423° to 1350° F.

Strength of insulations and bond to aluminum at cryogenic temperatures are discussed in appendix B, by Morgan P. Hanson; and a method of calculating one-dimensional transient heat conduction with variable thermal properties is presented in appendix C, by William Lewis. The authors wish to acknowledge the technical assistance and cooperation of the Plastics Division of Goodyear Aircraft Corporation, which fabricated most of the test models used herein.

APPARATUS AND PROCEDURE

Thermal-Conductivity Tests

Thermal conductivities of various insulation materials were determined over a range of cryogenic temperatures by two independent means: an electrically-heated conductivity meter that was totally immersed in liquid nitrogen, and an insulated tank from which the boiloff of cryogenic liquids was measured.

Conductivity meter. - The construction of the thermal-conductivity meter is shown in figure 1. The electric heater was fashioned from 0.001-by 1/8-inch Nichrome ribbon, pressed between two layers of pressure-sensitive glass tape. Thermocouples were centered on each face of the glass tape, and this assembly was encapsulated between two 0.003-inch layers of glass cloth impregnated with epoxy resin and then cured under vacuum-bag pressure. This produced a heater wafer of about 0.025-inch thickness, as shown in figure 1(b). One of these heater wafers was used for each material investigated, and one was tested bare for calibration purposes. Insulation material (usually 3/16 or 1/4 in. thick) was bonded to each face of the wafer and, to reduce edge effects, extended about 1/2 inch beyond the ribbon elements on all four edges (fig. 1(c)). The insulation was then externally sealed with a thin coating of epoxy resin or Mylar sheet. A finished specimen is shown in figure 1(d).

Some conductivity meters were equipped with two small pressure tubes extending about 1 inch into the insulation on either side of the heater wafer. These pressure probes were used with vacuum gages and pumps to measure and control the pressure within the insulation and to replace internal air with other gases.

The completed conductivity meters were each submerged in liquid nitrogen and thoroughly cooled to -321°F ; a small amount of electric power (a-c supply) was then applied. After equilibrium was reached (20 to 30 min), temperatures at the heater-insulation interface and input powers were recorded. This procedure was repeated for several stepwise power increases to cover the range of interest and back again to complete a hysteresis loop.

The thermal-conductivity data were calculated according to the following equation:

$$\frac{Q}{A} = \frac{k}{b}(\bar{t}_i + 321)$$

All symbols are defined in appendix A. In these calculations, a few simplifying assumptions are made. First, the thermal-conductivity factor k is determined as an "overall" value for the insulation composites tested, a lumped term that includes the effect of insulation material, bonding layer, seal layer, and, in samples with honeycombs, the cell walls and faces. Second, the heat flow near the center of the conductivity meter is assumed to be unaffected by heat losses through the edges. Based on the meter edge-to-face area ratios, the errors involved by neglecting edge losses are less than 10 percent. Third, the outer insulation surface in contact with the liquid nitrogen is assumed to be always at the nitrogen saturation temperature, -321° F. This assumption was adopted after experiments with an uninsulated wafer heater immersed in liquid nitrogen showed that the error involved in neglecting the temperature differential in the boiling liquid film was less than 2 percent over the range of test power densities. These error sources prevent the conductivity meter from having high precision; however, the errors are relatively small, and the simplicity of the meter design facilitated testing of a large number of materials.

Tank boiloff tests. - Thermal conductivities of insulations were also determined by measuring the volumetric rate of boiloff of cryogenic liquids from insulated tanks, as shown in figure 2. The cylindrical portion of the tank was covered with various test insulations, and the tank ends were insulated heavily with polyurethane foam to reduce heat losses through the ends. Exterior surface thermocouples were cemented to the test insulations in a vertical pattern as shown. The tank shown in figure 2 was annular (see cross section), with the central space completely filled with foamed-in-place insulation. To restrict air from penetrating into the insulation, the tank insulation exterior was completely covered with a bonded-on plastic film (Mylar) with tank ends sealed with blimp lacquer (table I). Pressure probes into the tank insulations were provided for monitoring and controlling the gas pressure and content inside the sealed insulation. In addition to the annular tank, a conventional hollow cylindrical tank was used for some tests. For rough indication of liquid levels, tank interior temperatures were measured by carbon resistors mounted on a vertical "dip-stick" that was part of the tank fill and vent-line assembly. The tanks were supplied from large pressurized Dewars, and the evolved gases were either vented or burned. All tank boiloff tests were conducted within a partial enclosure, which limited ground winds to less than 10 miles per hour.

In the boiloff tests, the general procedure was to fill and "top-off" the tank continuously for specified cold-soak periods (generally 30 to 60 min), then simultaneously close the inlet valve and switch the evolved gases through the gas meter while recording the initial readings. Thereafter, during the boiloff period, frequent readings were taken of the gas-meter dials, time, pressure and temperature at the gas meter, insulation surface temperatures, and tank interior temperatures. The tank boiloff data were then analyzed according to the method of reference 2. This method avoids the effects of tank-end heat losses by making use only of that heat-flow rate which varies linearly with height of the remaining liquid. Liquid level was calculated from boiloff rates and tank geometry.

Sealing Tests

Several materials for use as external seal coats over the insulations were tested at room temperature and at conservative anticipated operating temperatures near -100° F. The seal-test samples were made as follows: A flat sample of either composition corkboard A (table I) or a honeycomb core faced with phenolic glass-cloth laminate was bonded, except for a centered 2-inch-square area, to an aluminum plate. A tube was welded to the center of the back side of the plate. The seal material was applied to the entire front face of the sample. Following this, the four edges were sealed with a Mylar strip, leaving a net face area of about 18 square inches. Seal temperatures of -100° F were obtained by placing the sample face down in the vapors escaping from a partly filled Dewar containing liquid nitrogen.

To screen out unpromising seal coats at room temperature, samples were evacuated by a mechanical pump to less than 1 inch of mercury absolute and pinched off from the pump; if the subsequent pressure rise was greater than 1 inch of mercury per minute, the seal was arbitrarily considered inadequate. The remaining samples were tested with a mass-spectrometer helium-leak detector, which required the maintenance of a relatively low absolute pressure in the sample. For those samples that were unable to hold the low pressures required for helium-leak detection, pressure rise as a function of time after valving off the pumps was recorded.

High-Temperature Tests

The high-temperature tests of the tank insulations were conducted in a combustion-gas-flow tunnel shown schematically in figure 3. The test setup consisted of (1) a can-type jet-engine combustor as a hot-gas generator, (2) necessary piping to direct the hot gases to the test

section, and (3) a square tank filled with liquid nitrogen on which specimens of insulations were mounted. Air- and fuel-flow rates could be controlled independently to vary the gas temperature and velocity (measured downstream of the combustor). The combustion gas exhausted to the atmosphere downstream of the test tank.

The test tank was made of Inconel, 5.75 inches square and 10 inches long. Insulation specimens were bonded to the tank with an epoxy glass-cloth laminate (table I). Foamed plastic insulation was used on each end of the tank. The insulation specimens were 6 inches wide, 12 inches long, and about 1/4 inch thick. The specimens overlapped along the edges when assembled on the tank and completely covered the sides of the tank including the end insulation blocks. Metal corner and end strips protected the edges and ends of the insulation specimens from nontypical exposure to the high-velocity gas. Compensating strips were added to the walls of the tunnel to avoid abrupt changes in flow area (with consequent changes in Mach number). Thermocouples under the corner strips (between the strip and the surface of insulation) midway of the tank length were used to indicate the temperature of the insulation surface. This location of thermocouples avoided any disturbance to the insulation surface itself.

Mach number and pressure level of the gas flow over the insulations were determined by means of total-head probes and static-pressure taps near the downstream end of the test section. At this point, sonic gas velocities were obtained with gas temperatures of 550° F and greater. (Gas temperatures between 400° and 1500° F were easily attainable in the test setup.) By the use of high-pressure air, dynamic pressures in the gas stream of about 13 pounds per square inch were produced. These pressures are of the same order as those produced in flight trajectories at supersonic velocities and stratospheric altitudes.

During the high-temperature tests, the primary mode of operation consisted of sequences of stepwise increases in surface temperatures between successive heating cycles, with the starting temperature of each cycle being the chilled tank condition (insulation surface temp. of about -50° F). This mode of operation was used to cover the expected range of surface temperatures on a flight vehicle and to determine how the insulating materials deteriorate with temperature level. A secondary mode of operation consisted of a transient temperature cycle wherein the temperature level was increased with time at a predetermined rate to simulate an aerodynamic-heating condition.

At the beginning of each heating cycle, the tank was filled with liquid nitrogen. The tank was allowed to cold-soak until the temperatures of the outer surface of the insulation (under the corner strips) stabilized. The combustor was then ignited at a low flow rate and temperature.

For the stepwise temperature cycles, the flow rates of air and fuel were then increased so that the test surface temperature was reached in 10 to 20 seconds. The test temperature level was held for 30 seconds. Pressures, temperatures, and airflows were recorded during this time. Then the fuel flow was shut off and the airflow was decreased to cool the test section without further erosion of insulation surfaces that might have been damaged during the heating cycle. The temperature level of the heating cycles was progressively increased until all surfaces had failed. The procedure was the same for the transient-temperature cycle except that the temperature was increased linearly from 500° to 900° F in 40 seconds and then held at 900° F for 10 seconds. Visual inspections, photographs, and necessary repairs were made on the insulation surfaces and the instrumentation after each heating cycle.

RESULTS AND DISCUSSION

Thermal Conductivity

Conductivity of insulations will be presented in two groups: the insulations that are considered self-supporting and the filled-honeycomb insulations.

Self-supporting insulations. - Thermal conductivity as a function of the arithmetic mean insulation temperature (average of inner and outer surface temperatures) is presented in figure 4 for several materials (described in table I). These data were obtained from conductivity meters. The curves show a consistent and favorable temperature trend, the conductivities near -300° F being about 35 percent lower than those near -100° F. Conductivities, compared at a mean temperature of -200° F, range from 1.4 Btu/(hr)(sq ft)(°F/in.) for a dense structural material like phenolic glass-cloth laminate to 0.21 for foamed corkboard C. The conductivity values of the epoxy mastic show that the conductivity of epoxy laminate (in the same range as phenolic laminate) can be reduced by adding hollow glass spheres and chopped glass fibers to the resin. Such a material may have insulation value as a putty or filler around fittings, joints, and so forth.

Composition corkboard A and B and foamed corkboard C were tested in the as-received condition with nominal densities of 19, 16, and 12 pounds per cubic foot, respectively. Their thermal conductivities varied directly with density, as shown in figure 4, and thus agree well with published conductivities for natural corkboard (7 lb/cu ft), as given in reference 7. These published data were obtained with a guarded-plate apparatus for mean temperatures down to only about -115° F. Corkboard data for other densities but for mean temperatures above -50° F (refs. 8 to 10) also appear to agree with the data of figure 4.

To study the porosity of cork and the effect of internal gases on conductivity, air was evacuated from a sealed sample of corkboard A, and helium gas was introduced under slight positive pressure. The thermal conductivity increased about 15 percent because of the greater conductivity of helium than air. Subsequent replacement of the helium with CO₂ gas reduced the conductivity to about that of the initial air-filled case. A further reduction with CO₂ may have been possible if an effort had been made to remove carefully all residual helium. Similar helium-gas tests with corkboard B resulted in about a 50-percent conductivity increase; foamed corkboard C, 80 percent; and balsa wood, 85 percent. These increases vary inversely with density, as would be expected. This effect of helium is probably a function of contamination time (a few hours herein). In the conductivity tests, no effect of gas pressure in the samples was noted over a range from 1 atmosphere down to about 1000 microns of mercury absolute.

Filled-honeycomb insulations. - The thermal-conductivity-meter results for several honeycomb insulation panels are presented in figure 5. As shown in the sketch, the phenolic honeycomb cores were filled with various insulation materials and faced over with glass-cloth laminates (see table I). A considerable range in overall thermal conductivity is seen, depending on which filler material is used in the honeycomb cells. At -200° F mean temperature, the overall thermal conductivities vary from 0.32 Btu/(hr)(sq ft)(°F/in.) for Min-K 501 filler to 0.99 for a mastic of potassium titanate and epoxy, while air-filled honeycomb is 0.46. The overall conductivity values for honeycomb panels are higher than would be expected for the filler materials alone because of the relatively high heat conduction through the glass-cloth walls of the honeycomb cells. The conductivity values for filler materials alone were calculated from a heat-resistance concept of the cell walls in parallel with the filler materials and the honeycomb faces in series with the filled core. The only filler conductivity available for comparison at cryogenic temperatures is that of polyurethane foam, for which calculations yield values about 10 percent higher than those of reference 2.

Compared with air-filled honeycomb, Min-K 501 and polyurethane foam are useful for fillers, because their contributions to the total honeycomb panel weight are more than offset by their reductions in overall thermal conductivities. Based on the product of weight and conductivity, balsa and cork are considerably better than the best filled honeycombs tested.

Tank tests. - The thermal-conductivity results obtained from boil-off rates of liquid hydrogen and nitrogen in tanks insulated with corkboard A or foamed honeycomb are given in figure 6. The insulations were all initially sealed as shown in figure 2, except for the unsealed-corkboard case labelled in figure 6. The sealed-corkboard data from

boiloff measurements are about 20 percent lower than those obtained by the conductivity meter. This agreement is considered satisfactory in view of the different methods of conductivity determination.

The unsealed-corkboard conductivity (obtained with liquid hydrogen, fig. 6) averaged $0.33 \text{ Btu}/(\text{hr})(\text{sq ft})(^{\circ}\text{F}/\text{in.})$ at a mean temperature of -290°F . This is about 1.5 times the value for sealed cork. In the unsealed case, fresh ambient air is drawn into the insulation and liquefies. The combined effects of latent heat release and the presence of layers of liquid and frozen air inside the insulation result in significant increases in overall thermal conductivity. The 50-percent increase in conductivity for unsealed compared with sealed corkboard is probably some function of soaking time, the data herein being for 45 minutes' soak prior to boiloff.

More striking effects of air condensation are evident in the data of figure 6 for initially sealed foamed honeycomb. The data points are labelled in chronological order of testing for convenience of discussion. The first foamed-honeycomb test was made with liquid nitrogen and resulted in a conductivity of 0.36 at a mean temperature of -233°F . This compares favorably with the dashed line (air-filled, fig. 6) calculated from conductivity-meter measurements of figure 5, taking the different thicknesses into account. The second and succeeding foamed-honeycomb tests were made with liquid hydrogen. During the boiloff phase of the second test, audible crackling and wrinkling of the outer 0.010-inch phenolic glass-cloth skin occurred, confined to an area of about 36 square inches. Following this damage, pressure checks revealed that the foamed-honeycomb insulation was no longer sealed from ambient air. The apparent thermal conductivities for the second and third runs were 0.41 and 0.55, respectively, at mean temperatures of -305°F and -328°F . These marked increases in conductivity are attributed to a continually deteriorating seal of the foamed honeycomb with consequent increase in amount of air condensing and freezing. The third foamed-honeycomb run (conductivity 0.55) is 2.3 times the calculated dashed line on figure 6, or slightly more than half the conductivity of liquid nitrogen (indicative of the amount of liquid air in the insulation). In an effort to avoid this liquefaction of air within the insulation, the fourth foamed-honeycomb run was made with the internal air in the foam cells replaced by helium maintained at a pressure under 1 pound per square inch gage. The helium-filled foam resulted in an overall conductivity of 0.6 at -325°F . This compares with 0.53 calculated for helium-filled foamed honeycomb, as shown in figure 6.

All the foamed-honeycomb thermal conductivities were higher than those for corkboard, even when the latter was unsealed. Sealing of corkboard A is far less critical for the attainment of rated (handbook) thermal conductivity than is sealing of the kind of polyurethane foam used herein. Evidently, unless foams are truly unicellular and impermeable, their low

densities allow a considerable amount of ambient air to enter and condense and part of it to freeze in the insulation. Hence, for use on hydrogen tanks, insulations with large void contents will in general require the application and maintenance of a reliable, high-quality seal in order to realize rated thermal-conductivity performance.

Sealing

In view of the importance of a seal on the preceding results, the quality of the various sealing materials listed in table I was tested as described in APPARATUS AND PROCEDURE. Four of these materials, namely 0.001-inch-thick Mylar and Saran, or 0.005- to 0.010-inch-thick Neoprene and blimp lacquer were much better seals at both room and low temperature than all others studied. These four did not crack at low temperature (about -100° F), and in general the total-pressure increase was less than 500 microns of mercury after 10 minutes following an initial pressure of less than 60 microns of mercury absolute. Insignificant leakage of helium was detected with a mass spectrometer with all four of these coatings at a temperature of -100° F. All the other seals tested, although satisfactory for use at room temperature, crazed or cracked at low temperature and were discarded. No significant differences were noted in sealing quality over corkboard surfaces compared with phenolic glass-cloth laminate surfaces. Spray or brush coats less than 5 mils thick were generally undependable. For minimum weight and ease of fabrication, these results indicate the use of 1-mil Mylar or Saran sheets on plane or cylindrical surfaces and a 5- to 10-mil spray or brush-on coating of aluminum-filled blimp lacquer for complex surfaces and around fittings.

Strength of Bonded-On Insulations at Cryogenic Temperatures

It is desirable to bond insulation directly onto a rocket tank for reasons of simplicity and reliability. Unbonded insulations require complex attachments, straps, expansion joints, and sliding seals, and need considerable stiffness to resist aerodynamic flutter between attachments. With bonded insulations, none of these problems are present. However, bonded insulations cannot be jettisoned, and for some missions their weight becomes a critical item. A good bonded insulation should be light yet possess enough strength to hold together in the airstream, and to withstand pressurization and cryogenic chilling of the tank without buckling, delaminating, or losing its bond.

Several insulations have been tested for tensile and shear strengths at room and cryogenic temperatures, and the results are given in appendix B. Also given are bond strengths at liquid-hydrogen temperature between aluminum and epoxy glass-cloth laminate (used as bonding ply for insulations) for a variety of metal surface treatments. These results at low

temperatures may be summarized as follows: The tensile strength of corkboard A is around 275 psi; the various honeycomb strengths averaged around 500 psi; and the bond strength to aluminum in tension was at least 3000 psi for six different surface treatments of the aluminum. Thus, the bond strengths are far greater than the cohesive strengths of most suitable insulation materials.

In actual tanks, insulations are subjected to combined stresses in three directions because of tank shrinkage during filling. Such stresses are complex functions of the tank and insulation geometries and physical properties. Some insight into this problem was gained by cryogenically cooling various cylindrical tanks to which were bonded several test insulations. Results indicated that bonded insulations should be flexible so as to move with the tank during contraction and expansion. Corkboard A was satisfactory in this respect, as no structural failures occurred during any tank chill-down tests. However, with honeycomb-supported insulations, difficulty was experienced with external coverings of the sandwich panels. These outer faces separated from the honeycomb core and buckled outward whenever their stiffness was excessive. For example, outer coverings of 0.030-inch-thick phenolic glass-cloth laminate and 0.024-inch-thick phenolic asbestos felt buckled badly, whereas coverings of 0.010-inch phenolic glass-cloth laminate, 0.012-inch phenolic asbestos felt, and 0.020-inch Silastic-impregnated glass cloth appeared satisfactory, although marginal. In none of the tank chill tests did the bond fail between the metal tank and the insulation. These results were obtained with modest-sized tanks that were essentially unpressurized; with full-scale rocket tanks different results may be obtained because of scale effects, pressurization stresses, and fabrication difficulties.

High-Temperature Performance

The results of the high-temperature tests on corkboard, balsa, and faced-honeycomb insulation specimens are shown pictorially in figure 7. Most of the specimens were subjected to sequences of stepwise heating cycles ranging in surface temperatures from 300° to 1350° F (see key on fig. 7(a)). Three specimens were subjected to a transient-temperature cycle from 500° to 900° F (sequence Z). Both modes of operation are described in APPARATUS AND PROCEDURE. In all the heating tests, the damage to the specimens was greatest at the downstream end of the test section where the gas velocity was highest.

Corkboard. - Three types of corkboard (A, B, and C) were tested. These corkboards are described in table I. Corkboards A and B are granules of cork in an animal glue binder, whereas corkboard C is a foamed epoxy and cork mixture. As shown in figure 7(a), the effect of the temperature cycles on all the corkboard specimens was initially a charring of the outer surface. Eventually, the surface was roughened and pitted as the corkboard began to spall.

Specimens of corkboard A with three initial surface conditions were tested: uncoated, epoxy-coated, and phenolic varnish-coated. The uncoated corkboard A (specimen 1, fig. 7(a)) exhibited the least resistance to heat. After exposure at 800° F surface temperature (sequence S), the surface was severely charred and pitted, with a marked reduction in thickness. An epoxy brush coat (on specimen 2) afforded some protection to the surface. Specimen 3, coated with phenolic varnish, underwent the heating cycles of sequence T from 400° to 1350° F. No appreciable decrease in thickness of the specimen was apparent until the 1150° F cycle, during and after which the corkboard deteriorated rapidly. Other phenolic varnish-coated specimens of corkboard A were tested at the higher temperature heating cycles only (950° F and above). These specimens after testing were generally comparable to specimen 3 after the corresponding temperature cycle. This indicates that the rapid deterioration of the corkboard that started at the 1150° F temperature level is not a cumulative effect from the earlier lower-temperature cycles.

Corkboard B (specimen 4) is similar to corkboard A, except that it is lighter and has smaller granules. At temperatures up to 800° F (max. at which corkboard B was tested), there was no difference in the performance of these two corkboards. Because of the smaller granules in corkboard B, its surface after testing was not as rough as that of corkboard A.

Corkboard C (specimen 5) was the lightest of the corkboards tested. The test specimen failed rather abruptly during exposure at 550° F. This performance was in contrast to the gradual deterioration of corkboards A and B at much higher temperature levels. A phenolic varnish coating was tested on a corkboard C specimen also, but its effect was to cause surface cracks without providing any noticeable protective advantage.

Balsa. - Balsa with a phenolic varnish coating (specimen 6) remained intact through the 670° F cycle of sequence R. The specimen failed completely during the next higher temperature cycle of 800° F. Up to the time of failure, the surface of the specimen remained relatively smooth, with some minor cracking along the grain lines. An unvarnished balsa specimen failed during the 400° F cycle in a similar manner to the varnished specimen at 800° F. Thus, the varnish coating provided considerable surface protection for the balsa, but the balsa has a much lower temperature limit than corkboards A and B.

Faced honeycombs. - The faced-honeycomb specimens used in the high-temperature tests are described in table I, and the photographic results are given in figure 7(b).

Glass-cloth facings of epoxy (specimen 7) and phenolic (specimen 8) were tested in heating sequence Z (900° F max. surface temp.) while bonded to the honeycomb cores. After testing, it was evident that the epoxy

resin had softened and flowed out of the cloth on specimen 7, allowing the cloth to be delaminated and shredded by the force of the gas stream. The phenolic glass-cloth laminate (specimen 8) was still intact, with little more than dimpling of the surface over the honeycomb cells at the conclusion of sequence Z. The two outer layers of cloth were then mechanically removed from specimen 8, and the remaining layer (0.010-in. thick) survived a second heating sequence Z without surface damage.

Three other facings were tested on the honeycomb cores (specimens 9, 10, and 11). These specimens were covered with a 0.001-inch Mylar sealant film, which was destroyed during the first heat cycle of sequence T at 400° F. With bonded-on insulations, the loss of the sealing coat at around 300° to 400° F surface temperature is considered of secondary importance for high-acceleration, short-duration flights. The phenolic glass-cloth laminate (specimen 9), at the end of the 950° F cycle of sequence T, showed only surface dimpling over the honeycomb cells. During the 1150° F cycle, however, specimen 9 failed completely, including the epoxy inner bond between the honeycomb core and the tank. The asbestos-felt facing (specimen 10) showed only surface dimpling after exposure at 950° F and failed during the 1150° F cycle. The Silastic facing (specimen 11) separated partially from the honeycomb core during exposures at 550° and 700° F. The unseparated area remained intact through 850° F exposure, but the bond of the Silastic-impregnated glass cloth to the honeycomb core was questionable from the first separation until final failure during the 950° F cycle.

In all the tests on faced-honeycomb insulation with foam filler J (table I), the foam melted away steadily as the temperature levels increased. At the 900° to 950° F temperature level of sequences T and Z, the foam plastic in the cells was less than half its original thickness. In contrast with J foam filler, filler G is capable of withstanding higher soaking temperatures than the facings holding it in the cells.

In summary, for the conditions covered in these high-temperature tests, corkboard A (and probably B) coated with phenolic varnish has the advantage of being consumed gradually at high temperatures rather than failing suddenly and completely as did balsa and the faced-honeycomb insulations (as in specimen 7). The phenolic varnish afforded good surface protection for corkboards A and B and for balsa. Of the honeycomb facings, those containing phenolic resin were superior to those containing epoxy or Silastic. For the short times involved in the heating cycles of these tests, 1000° to 1100° F appears to be about the limiting temperature for the phenolic resins.

INSULATION FOR A SPECIFIC VEHICLE

So far, the various insulating materials and problems have been discussed separately, as much as possible. A practical insulation design would naturally make use of several materials to obtain the most desirable properties for each function to be performed. An actual insulation design will depend entirely on the specific vehicle and flight program involved. For an example, a vehicle and flight plan will be assumed so as to impose quite severe requirements on the insulation. A small hydrogen-oxygen rocket will be considered as the second stage of a high-acceleration vehicle. The compartmented second-stage tank will have an aluminum alloy skin limited by stress considerations to 100° F when pressurized in flight. The tank assembly will measure about 8 feet in length (lower 6 ft for hydrogen, upper 2 ft for oxygen) and 32 inches in diameter. The assumed flight plan is given in figure 8. The powered flight for both stages lasts 53 seconds, at which time the acceleration peaks at 13 g's, the altitude is 170,000 feet, and the velocity is nearly 10,000 feet per second. After the initial 22 seconds of flight, a maximum dynamic pressure of 25 pounds per square inch is reached, at which time the hydrogen-oxygen second stage is fired. Thus, sizable aerodynamic loads and frictional heating of the insulation can be expected.

An insulation design that should meet the stringent demands of the assumed vehicle and flight plan is shown in cross section in figure 9. Corkboard A is selected for its relatively low thermal conductivity, superior sealing properties and high-temperature characteristics, good flexibility, and adequate strength. The preferred bonding layer and external surface coatings are detailed on figure 9. The insulation thickness of 1/4 inch is an arbitrary compromise between weight and rate of fuel boiloff, which will be discussed later. This insulation design has an overall weight of 0.53 pound per square foot and a thermal conductivity of about 0.26 at -200° F.

To assess the performance of this corkboard insulation on the assumed rocket vehicle tank, calculated results will be given for both the ground-holding and flight phases of the vehicle.

Ground Performance

The calculated average external-surface temperature and the propellant vaporization rate with sealed corkboard A insulation bonded to the side walls of a 32-inch-diameter tank are presented in figure 10. These calculations are based on the following assumptions: The insulation is sealed against the influx of ambient air, and the external surface temperature is always above the air condensation temperature; the tank walls are at liquid bulk temperature; the insulating effect of an external frost

layer is not considered, nor is radiation or any phase-change heat-transfer process. The external heat-transfer coefficients are taken from references 11 and 12, considering free and forced convection of dry air. The curves in figure 10 cover a range of ground winds, ambient air temperatures, and corkboard thicknesses. Results are presented for tanks containing either liquid hydrogen or liquid nitrogen, with the latter somewhat representative of liquid oxygen. Included in figure 10 for comparison with calculations are experimental results for 1/4-inch-thick sealed corkboard A on a 24-inch-high tank (32-in. diam.) containing either liquid hydrogen or liquid nitrogen in an average environment of 80° F and a ground wind between 0 and 10 miles per hour.

The external surface temperature (from fig. 10) decreases rapidly with decreasing thickness. For example, with the hydrogen-filled tank in 80° F ambient air, the insulation surface temperatures vary from -108° F for 1/4-inch thickness to -214° F for 1/16-inch thickness in free convection (no ground wind). This 1/16-inch thickness is sufficient to keep the external surface temperature above the air condensation temperature. If the only change made is to a 20-mph ground wind, the surface temperatures are about 100° F warmer.

The calculated liquid-vaporization rates (equal to heat flux divided by the heat of vaporization) of figure 10 are presented per foot of tank length and apply only to the wetted or filled portion of the tank. For 1/4-inch thickness, hydrogen liquid-vaporization rates increase from 0.2 lb/(min)(ft) for 80° F ambient free convection to about 0.3 with a 20-mph ground wind. The effect of ground wind is more pronounced for the thinner insulations. The effect of increasing the thickness of insulation is one of diminishing returns. For example, the hydrogen vaporization rates at 80° F and a 20-mph wind are 0.72, 0.30, and 0.18 lb/(min)(ft) for 1/16, 4/16, and 8/16 inch thick, respectively. Nitrogen liquid-vaporization rates are about 1.9 times those for hydrogen; but, on a volume basis, hydrogen vaporizes at about 6 times the nitrogen rate.

For the tested 1/4-inch corkboard A near 80° F and ground wind between 0 and 10 mph, the average experimental liquid-vaporization rates are 0.18 lb/(min)(ft) for hydrogen and 0.35 for nitrogen; the measured surface temperatures are about -54° and -44° F, respectively. The experimental values are close to those calculated, indicating that errors due to the assumptions involved were largely compensatory.

With a full hydrogen tank insulated with 1/4-inch sealed corkboard A, the volumetric vaporization rates per minute are about 0.74 and 0.82 percent of tank volume in 40° and 80° F ambient free convection, respectively, and about 1.2 percent in 80° F ambient with a 20-mph ground wind. These percentages would decrease for larger-diameter tanks because of their smaller area-to-volume ratios.

Flight Performance

To assess the performance of 1/4-inch corkboard A insulation in flight, an analysis was made of the thermal transients through the insulation, accounting for the assumed vehicle flight plan, the thermal capacity of the insulation, and the variation of specific heat and thermal conductivity with temperature. The analysis is presented in appendix C, and the results are summarized in figure 11, wherein heat flux and surface temperature are given as functions of flight time. Of the heat-flux lines, the highest line shows the total heat flux delivered to the external surface of the insulation from the airstream by convection. The next lower line indicates the net heat flux into the insulation, and the shaded region between these lines represents the portion of the total heat flux that radiates away. The shaded area at the bottom of figure 11 represents the heat that actually reaches the liquid hydrogen through the insulation and tank wall. Just before the end of powered flight, the net heat flux into the liquid is at a rate only double the value while on the ground (zero flight time). Most of the aerodynamically generated heat is either radiated away or stored in the insulation. The heat that actually goes through the insulation and into the remaining liquid hydrogen in this example will vaporize only about 3/4 of 1 percent of the initial liquid volume during the 53 seconds of powered flight.

Referring to the surface-temperature curve of figure 11, the corkboard external temperature peaks at about 1220° R (760° F), while the innermost layer and the wetted tank wall remain at 37° R (-423° F). From the data in figure 7, it is evident that little ablation of the cork exterior will result from these flight temperatures.

In summary, the performance of this corkboard A insulation, for the specific example chosen, is more than adequate to meet the severe requirements of the rocket flight, and further study should help in optimizing the weight in terms of mission performance.

COMMENTS AND RECOMMENDATIONS

Although corkboard A is preferred for tank insulation for the assumed vehicle and flight plan, it does not represent an ideal solution for all vehicles and missions. For other flight plans or missions, the design compromises among thermal conductivity, sealing, high-temperature performance, strength and flexibility at low temperature, weight, reliability, and so forth, may be significantly different.

Among the corks, corkboard B will provide a smoother aerodynamic surface and be lighter than corkboard A, but it is more porous and thus

subject to increased sealing problems. Foamed corkboard C is the lightest but also the most porous and most subject to high-temperature damage; however, this latter characteristic might be used to advantage by tailoring it to ablate away in a flight-programmed manner. Compositions of cork granules and resins or binders different from those studied herein could conceivably improve a particular design even more.

Of the other materials, the lightest-weight design would probably be balsa wood, although flexibility and sealing would present problems not completely studied herein. Lightweight plastic-foam insulations may be advantageous for the low-acceleration vehicles; but their strength, high-temperature resistance, and sealability must be demonstrated. Finally, the insulation-filled phenolic honeycombs might be desirable for smooth, durable surfaces on recoverable boosters, for example.

Although this investigation was confined to externally bonded insulations for atmospheric flight, some of the results and data should be helpful in the design of other tank insulation types, such as internal, integral, and jettisonable insulations. On the other hand, for missions requiring fuel storage in space, further study of the radiation properties of insulation surfaces would be required.

SUMMARY OF RESULTS

For the materials and test conditions covered in this investigation of bonded and sealed external tank insulations for use during ground holding and atmospheric flight of liquid-hydrogen-fueled rockets, the following principal results were obtained:

1. For high-acceleration vehicles with large aerodynamic heating loads, the most reliable insulation material is commercial composition corkboard, having a density in the range between 16 and 20 pounds per cubic foot. Two other materials may be suitable, but appear marginal with respect to structural integrity at both low and high temperatures; these are (a) phenolic honeycomb filled with low-density insulation sandwiched between thin glass-cloth facings, and (b) balsa wood.

2. Overall thermal conductivities of several tank insulation designs were obtained over a range of cryogenic temperatures. For comparison at a mean temperature of -200°F , the following conductivities resulted: foamed corkboard, $0.21 \text{ Btu}/(\text{hr})(\text{sq ft})(^{\circ}\text{F}/\text{in.})$; balsa, 0.23; composition corkboard, 0.24 to 0.26; foam-filled honeycomb sandwich, 0.38; air-filled honeycomb, 0.46.

3. Insulations must be well sealed from the influx and condensation of ambient air if rated thermal conductivity is to be realized and maintained. For example, unsealed composition corkboard on a hydrogen tank yielded a thermal conductivity 50 percent higher than the rated value obtained by corkboard sealed with a 0.001-inch-thick plastic sheet.

Polyurethane foam-filled honeycomb insulation with small leaks in the seal yielded conductivity values as much as 130 percent higher than its rated value.

4. Approximate external surface temperatures at which various insulation designs may be expected to fail because of aerodynamic heating were determined, such as: composition corkboard, 1100° to 1350° F; phenolic honeycomb, 1100° F; balsa, 700° F; foamed corkboard, 450° F. In contrast to the others, composition corkboard failed gradually in thickness over a range of elevated temperatures, retaining a fairly smooth, though charred, external surface.

5. At liquid-hydrogen temperature, tensile strengths of various insulations and their bond to aluminum (using epoxy glass-cloth laminate) were measured. The bond strengths (3000 psi or more) were far greater than the cohesive strengths of the insulations (av. of 500 psi).

6. A calculated example of an assumed small, high-acceleration, two-stage, hydrogen-fueled rocket vehicle with tank insulation of 1/4-inch-thick composition corkboard yielded the following: peak dynamic pressure, 25 pounds per square inch; peak surface temperature, 760° F; fuel boiloff from aerodynamic heating during flight, 3/4 of 1 percent of initial volume; fuel boiloff or "topping rate" while on the ground, about 1 percent of full tank volume per minute.

Lewis Research Center

National Aeronautics and Space Administration

Cleveland, Ohio, July 25, 1960

APPENDIX A

SYMBOLS

A	area (equal to twice area of rectangle drawn around outermost ribbon elements in conductivity meter), sq ft
b	thickness, in.
C	heat capacity of C layer in appendix C, Btu/(sq ft)(°R)
h_{ex}	external convective heat-transfer coefficient in appendix C, Btu/(sec)(sq ft)(°F)
k	thermal conductivity, Btu/(hr)(sq ft)(°F/in.)
Q	heat-flow rate (equal to total electric power dissipated in conductivity meter), Btu/hr
q	heat flux in appendix C, Btu/(sec)(sq ft)
q_r	radiation heat flux in appendix C, Btu/(sec)(sq ft)
T	absolute temperature in appendix C, °R
\bar{t}_i	average temperature of two interface thermocouples in conductivity meter, °F
U	thermal conductance of U layer in appendix C, Btu/(sec)(sq ft)(°R)
x	distance in appendix C, in.
θ	time constant defined in appendix C, sec
τ	time in appendix C, sec
Subscripts:	
1,2, ... n	reference planes (applies to C and T), in appendix C
1,2;2,3; ...	intervals between reference planes (applies to U and q), in appendix C

APPENDIX B

STRENGTH OF INSULATIONS AND BOND TO ALUMINUM AT CRYOGENIC TEMPERATURES

By Morgan P. Hanson

In bonding insulation directly to rocket propellant tanks, both the bond between the insulation and metal tank and the insulation composite must have sufficient strength to withstand stress conditions influenced by environmental factors. Probably the most severe stress condition is due to the difference in thermal contraction of the insulation and the tank material. High g forces inherent in rocket and missile operations also increase the loads on the insulation. The present investigation is limited to an aluminum tank material, although it is recognized that the tank material can affect the performance of insulation, particularly that due to thermal effects.

To simulate operational temperature conditions, tensile tests were made of insulation composites and of bonds in liquid hydrogen, with a few tests at liquid-nitrogen and room temperature.

Test Specimens

The insulation composites for the strength tests were made of phenolic honeycomb and of composition corkboard A (table I). The honeycomb composites had cores 0.15 inch thick, filled with either polyurethane foam or air. Cores with 3/16- and 3/8-inch cells were investigated. The honeycombs were faced with glass cloth impregnated with either a phenolic or an epoxy resin. The cork composites were of corkboard A nominally 1/4 inch thick. Glass cloth was used to face the composites between the 1-square-inch surfaces of a pair of aluminum blocks. The composites were bonded with either phenolic or epoxy resins to surfaces that were either wire-brushed or vapor-blasted.

In the bonding tests, several different procedures were used to prepare the bonding surfaces. Many of the surfaces were given an abrading treatment that consisted of either wire-brushing, chemical film, vapor-blast, or anodizing. Some tests were made with only a degrease treatment. Other tests were made with primers in conjunction with the bonding media. The bond ply described in table I was used to face the bonding surfaces.

Apparatus

The hydrogen tests were made in a cryostat designed for mounting in a tensile loading fixture. The apparatus is shown in figure 12. The specimen assembly, in position for testing, is pin-supported at the base of the cryostat. A bellows, providing a flexible seal between the cryostat and the upper loading rod, allows loading of the specimen without hydrogen boiloff escaping around the test apparatus. The sealed cryostat is vented to the atmosphere. With the specimen at liquid-hydrogen temperature, load was applied by means of a hydraulic ram supplied by a remote pressurized oil system. The load was measured with a strain-gage load cell and recorded on a recording potentiometer. A commercial universal testing machine was used for test at temperatures other than that of liquid hydrogen. A range of test temperatures, besides ambient room and liquid-nitrogen temperatures, was obtained for some tests by using either dry ice, dry ice and kerosene bath, ice bath, or heated water bath.

Results

The ultimate tensile and shear strengths of a number of insulation composites, determined in a range from room temperature to liquid-hydrogen temperature, are given in table II. The tensile strengths of the honeycomb composites were lower at liquid-hydrogen temperature (340 to 700 psi) than at room temperature (448 to 885 psi). The loss in strength at liquid-hydrogen temperature can possibly be attributed to the biaxial stress condition due to difference in thermal contraction of the composite and the aluminum loading block. Differences in strength between the foam-filled and air-filled honeycombs were not significant. The 3/8-inch-cell honeycomb was weaker than the 3/16-inch. The shear tests gave strengths on an average lower than the tensile strengths. In all the honeycomb tests the fracture was between the honeycomb core and the glass-cloth facing; hence the strength of the honeycomb composite depended on the bond between the core and the glass-cloth facing. Generally, the strengths of the phenolic and the epoxy glass-cloth faces on honeycomb cores were about equivalent. The tensile strengths for a mastic of epoxy resin and potassium titanate, suitable as a filler material around fittings and joints, ranged between 2250 and 3550 psi.

Table II shows that the tensile strength of the corkboard A was lower than that of the honeycombs and varied with the temperature. A plot of corkboard A tensile strength as a function of temperature is shown in figure 13. The corkboard tensile strength is seen to increase appreciably from room temperature (about 60 psi) down to -100°F (about 300 psi), with very little additional strength change from -100°F down to liquid-hydrogen temperature. The increase in the tensile strength of corkboard A at reduced temperatures is typical of most materials. The leveling off

characteristic of the strength below -100° F can possibly be explained by the fact that corkboard becomes embrittled at the low temperatures. Above room temperature, the tensile strength dropped to about 25 psi at 150° F. The observed intergranular fracture was quite pronounced at 150° F, indicating a limitation of the binder in the composition corkboard at elevated temperatures. (Limited tensile tests of natural cork taken from bottle stoppers revealed somewhat higher strengths at temperatures between 50° and 150° F.)

In designing insulation to be bonded directly onto a metal tank, the chief consideration is the shrinkage of the tank when it is chilled with cryogenic liquid. The shrinkage in aluminum is about $1/3$ greater than in the stainless steels and is about 7 percent greater when cooled with liquid hydrogen than when cooled with liquid nitrogen. The total linear shrinkage of aluminum, from room temperature to liquid-hydrogen temperature, is about 0.4 percent. Epoxy resin reinforced with glass fibers has been shown almost to match the contraction rate of aluminum and also is a strong adhesive down to low temperatures (refs. 3 and 13). The strength of the bond of epoxy glass-cloth laminate to aluminum, however, is greatly affected by the condition and treatment of the metal surface. It is important for a reliable bond that the epoxy bonding layer be applied soon after the surface treatment process (within a day). These surface effects were determined by tensile-strength tests and are shown in figure 14. The breaking tensile strengths for these various surface treatments were determined with the majority of specimens submerged in liquid hydrogen, indicated by the letter H. A few specimens were tested at liquid-nitrogen and room temperature, but no consistent temperature trends were established. The results range from a bond strength of about 1100 psi for "degrease only" to more than 5000 psi for vapor blast. However, several of these common surface treatments yield bond strengths of at least 3000 psi, which is far greater than the strength of most suitable insulation materials.

APPENDIX C

STEP METHOD OF APPROXIMATE NUMERICAL CALCULATION OF ONE-DIMENSIONAL
TRANSIENT HEAT CONDUCTION WITH VARIABLE THERMAL PROPERTIES

By William Lewis

The step method of solving transient heat-conduction problems is very simple in principle and flexible in application (ref. 14). It is especially useful for obtaining approximate numerical solutions in cases in which the variation of thermal conductivity with temperature is too large to be neglected, and approximate methods based on the diffusion equation such as those of Schmidt (described in ref. 14) and Dusenberre (ref. 15) cannot be used.

The problem was to determine temperature and heat flux as a function of time and position in a 1/4-inch-thick slab of insulation on the side wall of a rocket fuel tank. The temperature of the inside surface of the slab was assumed constant. The external heat-transfer coefficient and the driving temperature (ambient air temp. plus kinetic rise) were given as a function of time. The thermal conductivity and specific heat of the slab material were given as functions of temperature, and the density was assumed constant.

Representation of Slab by Laminated Model

In order to apply finite-difference equations to the analysis of heat flow in a continuous slab, it is necessary to represent the slab approximately by a model consisting of a series of layers. In this problem, the outer layers were chosen as thin as practicable in order to obtain a reasonably close approximation to the true surface temperature. In the inner portions of the slab, where more sluggish temperature changes were anticipated, a larger layer thickness was selected. Thus, a series of reference planes, identified by the numbers 1 to 9, was chosen as indicated in figure 15. Plane 1 is located at the outside surface of the slab and plane 9 at the inside surface. Planes 1 to 5 are separated by a distance interval Δx of 1/12 of the slab thickness (1/48 in.) and planes 5 to 9 are separated by twice that distance (1/24 in.).

The model consists of a series of alternate layers of two types, C layers and U layers (fig. 15(d)). The U layers, located between the reference planes, have finite heat conductances $U_{1,2}$, $U_{2,3}$, and so forth, but zero heat capacity. The C layers, located in the reference planes, have finite heat capacity and zero thickness. The heat capacities, designated C_1 , C_2 , and so forth, include the heat capacity of the portion of

the slab on each side of the reference plane out to a point midway between it and the adjacent reference plane. Both C and U are functions of temperature; C_n is determined by the value of T_n , and $U_{n,n+1}$ is determined by the value of $1/2(T_n + T_{n+1})$. Values of C and U used in the calculation are shown in figure 16.

Boundary and Initial Conditions

The boundary conditions were as follows:

(1) $T_9 = 37^\circ \text{R}$ for all values of time τ .

(2) The external heat-transfer coefficient h_{ex} and the driving temperature T_0 are given in figure 17 as functions of τ . These curves are based on an analysis of the flight plan (fig. 8) by the methods described in reference 16.

(3) The radiation flux q_r was calculated for an emissivity of 0.9. The initial temperature distribution was found by trial calculations using $h_{\text{ex}} = 0.0012 \text{ Btu}/(\text{sq ft})(\text{sec})(^\circ\text{R})$ and $T_0 = 530^\circ \text{R}$ and making $q_{0,1} = q_{1,2} = q_{2,3}$, and so forth.

Calculation of Heat Flux and Temperature Changes

Let T_1, T_2, T_3 , and so forth, represent the temperature at time $\tau = \tau_0$; and let T'_1, T'_2, T'_3 , and so forth, represent the temperature a short time later at $\tau = \tau_0 + \Delta\tau$.

Values of heat flux across the U layers at τ_0 are given by

$$\left. \begin{aligned} q_{1,2} &= U_{1,2}(T_1 - T_2) \\ q_{2,3} &= U_{2,3}(T_2 - T_3) \end{aligned} \right\} \quad (C1)$$

and so forth. The heat flux into the outside surface at τ_0 is equal to the external convective heat transfer minus the net outward radiation:

$$q_{0,1} = h_{\text{ex}}(T_0 - T_1) - q_r \quad (C2)$$

The rate of change of temperature of the C layers at τ_0 is given by

$$\frac{dT_1}{d\tau} = \frac{q_{0,1} - q_{1,2}}{C_1}$$

$$\frac{dT_2}{d\tau} = \frac{q_{1,2} - q_{2,3}}{C_2}$$

and so forth. If $\Delta\tau$ is sufficiently small, the average rate of change of temperature during the interval $\Delta\tau$ is approximately equal to the rate at τ_0 . Thus, the temperatures at $\tau_0 + \Delta\tau$ are

$$\left. \begin{aligned} T'_1 &= T_1 + \frac{\Delta\tau}{C_1}(q_{0,1} - q_{1,2}) \\ T'_2 &= T_2 + \frac{\Delta\tau}{C_2}(q_{1,2} - q_{2,3}) \end{aligned} \right\} \quad (C3)$$

and so forth.

Heat flux and temperature as functions of time and position were determined by repeated applications of equations (C1), (C2), and (C3).

Selection of Time Step

Values of $\Delta\tau$ consistent with the layer thicknesses were chosen with reference to the time constants defined as follows:

$$\beta_1 = \frac{C_1}{h_{ex} + (dq_r/dT_1) + U_{1,2}} \quad \text{for the outer layer}$$

and

$$\beta_n = \frac{C_n}{U_{n-1,n} + U_{n,n+1}} \quad \text{for the interior layers}$$

Since the value of β is an approximate indication of the minimum time interval of significance in the calculated results (because of finite layer thickness), there is no advantage in taking $\Delta\tau$ much smaller than β . On the other hand, use of a time step larger than β may lead to a kind of instability in the stepwise calculation process, with values of

ΔT becoming alternately too large and too small in a divergent manner. Thus, the optimum relation between time and distance intervals should be expressed in terms of a relation between β and $\Delta\tau$. This optimum relation cannot be established without further investigation, but the following empirical rules for the selection of $\Delta\tau$ have been found useful:

(1) Stability of the calculation is assured if $\Delta\tau$ is not greater than the smallest value of β .

(2) Instability is likely to develop if $\Delta\tau$ exceeds β for three or more adjacent layers.

Values of β for selected times and values of $\Delta\tau$ used in the calculation are shown in the following table:

Flight time, τ , sec	β_1 , sec	β_2 , sec	β_4 , sec	β_5 , sec	β_6 , sec	β_8 , sec	$\Delta\tau$, sec		
							Layer 1	Layers 2 to 4	Layers 5 to 8
0	1.0	1.2	1.1	2.1	3.6	2.1			
0 to 15							0.5	0.5	2
7.5	0.3	1.4	1.2						
15	0.3	1.6	1.3	2.3	3.7	2.1			
15 to 24							0.5	1	2
24	0.7	1.8	1.4	2.5	4.0	2.2			
24 to 60							1	1	2
60	1.6	2.0	1.9	3.6	6.1	3.2			
60 to 70							2	2	2
70 to 79							3	3	3

A considerable saving in labor was accomplished by using a longer time step for the thicker layers. The intermediate values of temperature required to calculate heat flux by equation (C1) were obtained by linear interpolation. Values of $\Delta\tau$ used in the calculation were generally smaller than β except for the outer layer. Since no difficulty was encountered with $\Delta\tau$ larger than β for the outer layer, use of $\Delta\tau$ larger than β for four consecutive layers was attempted at the end of

the program ($\tau = 70$ sec). Under these conditions a noticeable divergence developed in only three steps of calculation.

Results

The calculated temperature of the C layers and heat flux across the U layers are shown in figures 18 and 19. The maximum temperature of the outer surface was 760° F. The surface temperature exceeded 500° F for 35 seconds, and the maximum depth of penetration of temperatures of 500° F or higher was 15 percent of the insulation thickness. The maximum temperature at the middle of the layer was 130° F. Integration of the heat-flux curves of figure 19 shows that the total heat entering the outside surface of the insulation during the 53 seconds of powered flight was 51.6 Btu per square foot. Of this total, 45 Btu per square foot was stored in the insulation, and one-half of this was contained in the outer one-sixth layer. Thus, only 6.6 Btu per square foot reached the inside surface of the insulation and entered the liquid.

REFERENCES

1. Scott, Russell B.: Cryogenic Engineering. D. Van Nostrand Co., Inc., 1959.
2. Anon.: Insulation for Liquid Oxygen Tanks. Rep. 5A229, NBS, Feb. 29, 1956.
3. McClintock, R. M., and Hiza, M. J.: Epoxy Resins as Cryogenic Structural Adhesives. Rep. 5093, NBS, June 20, 1957.
4. Eppinger, C. E., and Love, W. J.: Bonding Plastic to Metal for High Strength at Low Temperatures. Proc. 1958 Cryogenic Eng. Conf., Jan. 1959, pp. 123-131.
5. McClintock, R. M.: Mechanical Properties of Insulating Plastic Foams at Low Temperatures. Proc. 1958 Cryogenic Eng. Conf., Jan. 1959, pp. 132-140.
6. Ruccia, F. E., and Mohr, C. M.: Atmospheric Heat Transfer to Vertical Tanks Filled with Liquid Oxygen. Proc. 1958 Cryogenic Eng. Conf., Jan. 1959, pp. 307-318.
7. Wilkes, G. B.: Thermal Conductivity, Expansion, and Specific Heat of Insulators at Extremely Low Temperatures. Refrigeration Eng., vol. 52, no. 1, July 1946, pp. 37-42.

8. McAdams, W. H.: Heat Transmission. Third ed., McGraw-Hill Book Co., Inc., 1954, pp. 449, 454.
9. Wilkes, G. B.: Heat Insulation. John Wiley & Sons, Inc., 1950.
10. Rowley, F. B., Jordan, R. C., and Lander, R. M.: Thermal Conductivity of Insulating Materials at Low Mean Temperature. Refrigeration Eng., vol. 50, no. 6, Dec. 1945, pp. 541-544.
11. Eckert, E. R. G.: Introduction to the Transfer of Heat and Mass. McGraw-Hill Book Co., Inc., 1950, pp. 24; 142.
12. Jakob, Max: Heat Transfer. Vol. I. John Wiley & Sons, Inc., 1949, pp. 530.
13. Frost, William M.: Strengths of Structural Adhesives at Temperatures Down to Minus 424° F. TR 59-260, WADC, Nov. 1959.
14. Ingersoll, L. R., Zobel, O. J., and Ingersoll, A. C.: Heat Conduction with Engineering and Geological Applications. McGraw-Hill Book Co., Inc., 1948.
15. Dusenberre, G. M.: Numerical Methods for Transient Heat Flow. Trans. ASME, vol. 67, no. 8, Nov. 1945, pp. 703-710; discussion, pp. 710-712.
16. Kramer, John L., Lowell, Herman H., and Roudebush, William H.: Numerical Computation of Aerodynamic Heating of Liquid Propellants. NASA TN D-273, 1960.

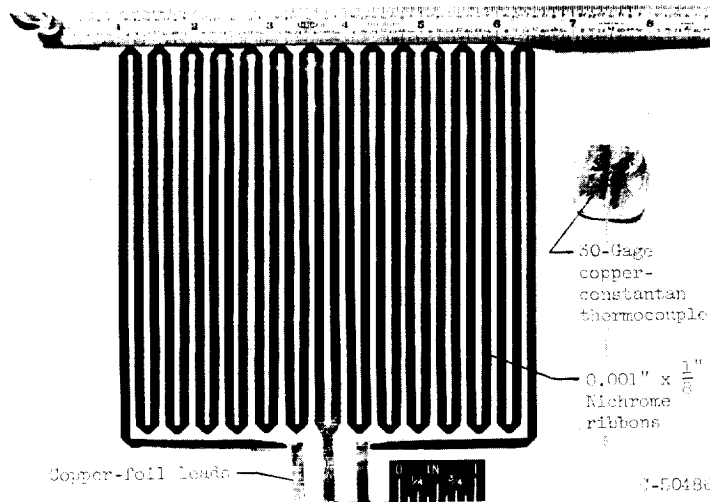
TABLE I. - MATERIALS TESTED

	Material	Description	Density, lb/cu ft	Nominal thickness, in.	Test type			
					Thermal conduc- tivity	Strength (see also table II)	Seal	High temper- ature
Self- supporting insulations	Composition corkboard A	Armstrong Cork # 9530	18-20	1/4	p.7, f.4,6	p.10,20, f.13	p.8,10, f.6	p.11,f.7
	Composition corkboard B	Armstrong Cork # 9520	~18		p.7,f.4			
	Foamed corkboard C	Armstrong Cushion Cork	~12	1/2				p.12,f.7
	Balsa wood	Balsa Ecuador, AA grade	8-10					
	Phenolic laminate	#181 glass cloth, Pyroreg AC-3 (Cordo Chemical)	115					
Filled- honeycomb insulations	Waterglass laminate	Synthetic mica, Crystal-M (Minn. Mining & Mfg.)	49	1/8				
	Epoxy mastic	Epon 815 (Shell), Glass spheres (Sohio), and glass fibers	40	5/16				
	Honeycomb core	3/16- and 3/8-in. cell, phenolic glass cloth	9	0.15 & 0.25	p.8,f.5	p.11,21		p.12,f.7
	Fillers: D	Air						
	E	Potassium titanate-epoxy mastic						
External- surface seals	Pliobond	Dry potassium titanate (duPont)	20					p.13,f.7
	Blimp lacquer	Min-k 1301 } Johns-Manville	10					
		Min-k 501 } Polyurethane foam	4		p.8,f.5,6	p.21 p.11,21	p.9,f.6	p.12,f.7
	Neoprene spray	#181 glass-cloth epoxy (Epon 820)		.010 & .030				
	Phenolic varnish P	#181 glass-cloth phenolic (Pyroreg AC-3)	115	.010 & .030				
Bond ply	Butyrate dope	Phenolic-asbestos felt (Raybestos- Manhattan)		.012				
	Epoxy	Silastic (Dow Corning) impregnated glass cloth		.020				
		Uncoated sheet (duPont)		0.001			p.10	p.13,f.7
		Adhesive (Goodyear Tire)		.001				
		Rubber-based, Al-filled lacquer (Goodyear Tire #1837C)		.005-.010				
Bond ply	Neoprene spray	Erosion coat as used on radomes		.005-.010				p.12,f.7
	Phenolic varnish P	Tuf-On 747-S (Brooklyn Paint and Varnish Co.)		~.002				
	Butyrate dope	Epi-Rez (Jones-Dabney Co.)		~.005				p.12,f.7
	Epoxy			~.005				
	Epoxy glass-cloth laminate	#181 glass cloth (Epon 820)		0.010		p.10,22, f.14		p.13

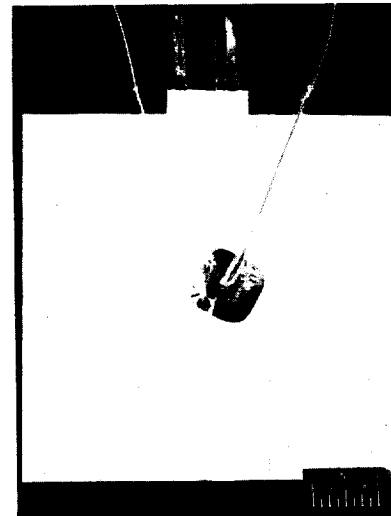
TABLE II. - ULTIMATE STRENGTH OF INSULATION COMPOSITES

Glass-cloth faces of:	Test	Temperature, °F	Honeycomb type		Honeycomb strength, psi	Composition corkboard A, psi
			Cell, in.	Fill		
Three-ply high-temperature phenolic (Pyroreg)	Tensile	-423	3/16 3/16	Foam Air	490 600 700 470 635 650	
		-423 70	3/8 3/8	Air Air	340 385 840	
Three-ply phenolic	Tensile	-423 70	3/16 3/16	Foam Foam	420 456 448	
One-ply epoxy (Epon 820)	Tensile	-423 70	3/16 3/16	Foam Foam	653 653 870	
		-423 70	3/8 3/8	Air Air	345 362 560	
		70 -321 -423				55 60 62 65 250 285 290 252 280 298 310
No cloth ply, Epon 820 resin	Tensile	-423				120 280 298
No cloth ply, Pliobond	Tensile	-423				135 260
One-ply epoxy-phenolic	Tensile	-423 70	3/16 3/16	Foam Foam	510 560 885	
One of three-ply high- temperature phenolic, other of one-ply epoxy	Lap shear	-423 70	3/16 3/16	Foam Foam	538 538 325	
		70 -423	3/16 3/16	Air Air	480 387 430	

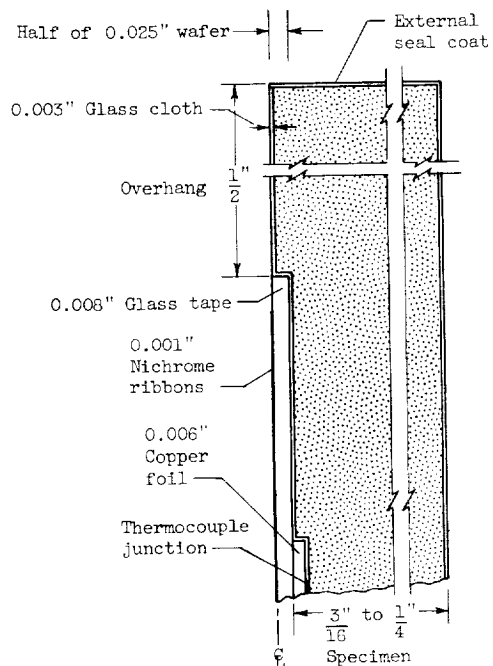
Structural filler material	Test	Temp.	Strength, psi
Potassium titanate-epoxy mastic	Tensile	-423 70	2250 3550 2300



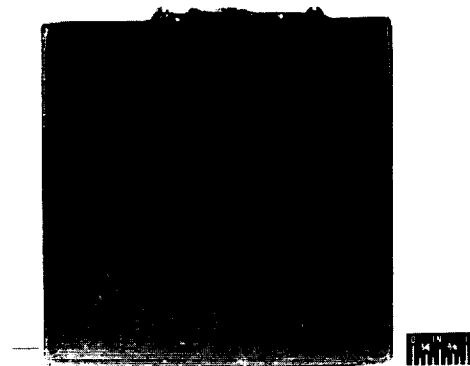
(a) Nichrome ribbon heater and detached thermocouple.



(b) Ribbon heater encapsulated in glass cloth, thermocouples in place.

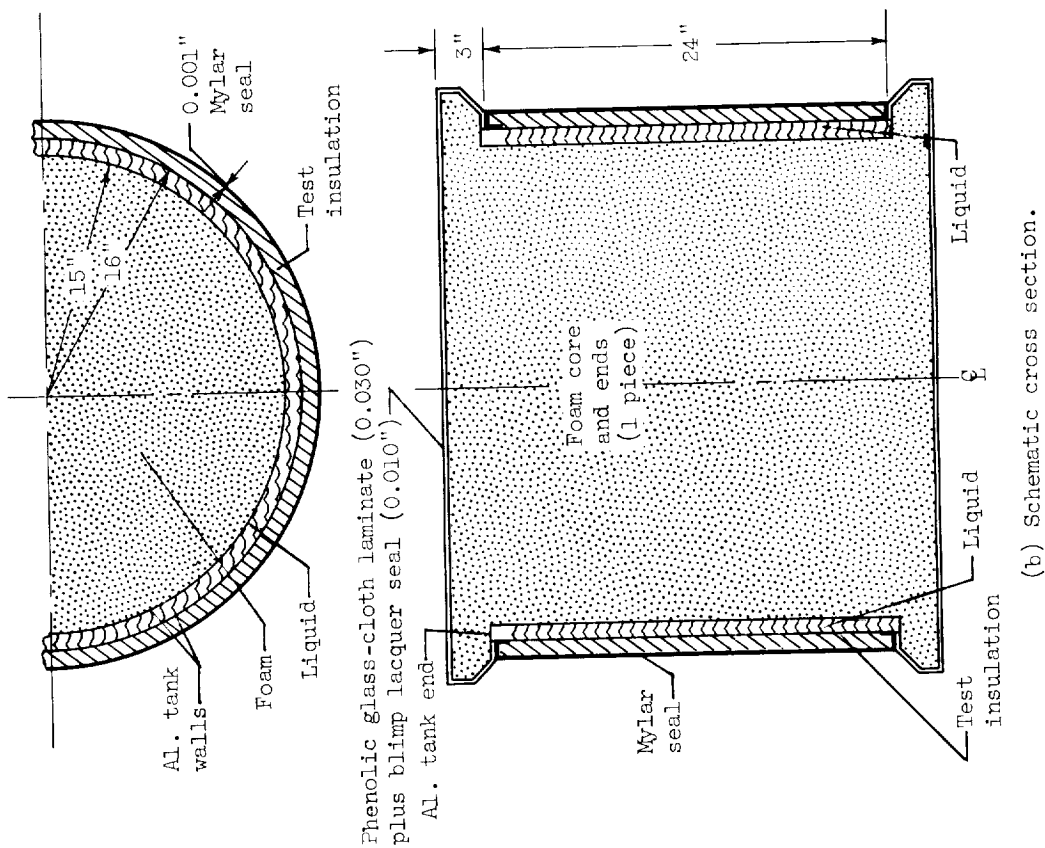


(c) Typical schematic cross section.

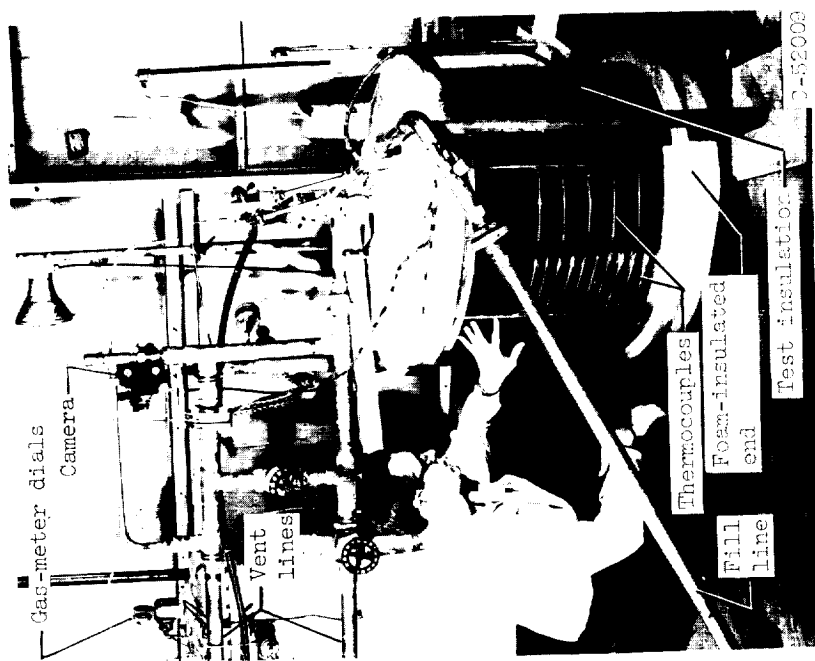


(d) Full assembly for insulation specimen.

Figure 1. - Construction of thermal-conductivity meter.



(b) Schematic cross section.



(a) Overall view.

Figure 2. - Boiloff tank and test equipment.

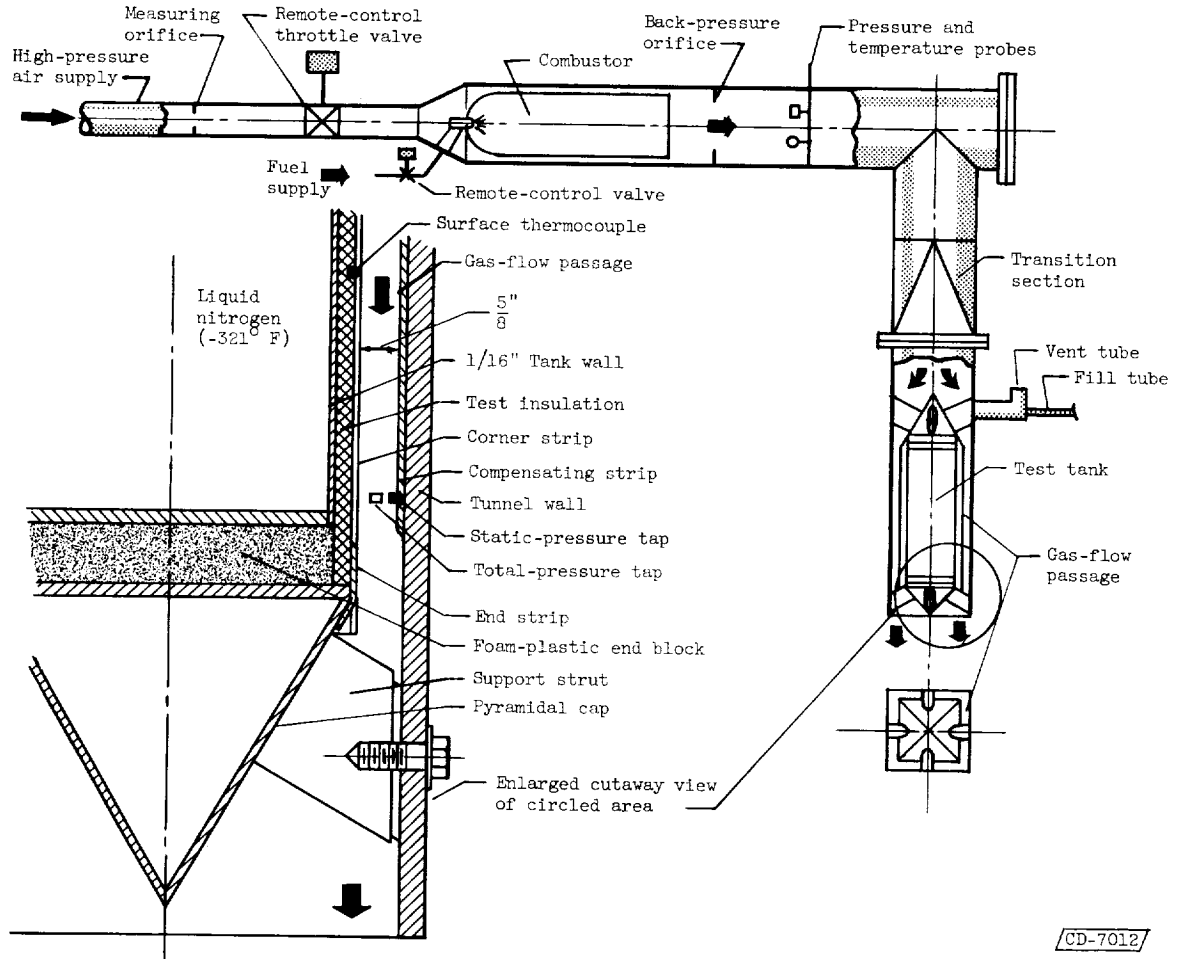


Figure 3. - Schematic diagram of setup for high-temperature tests of insulations on liquid-nitrogen-filled tank in hot-gas-flow tunnel.

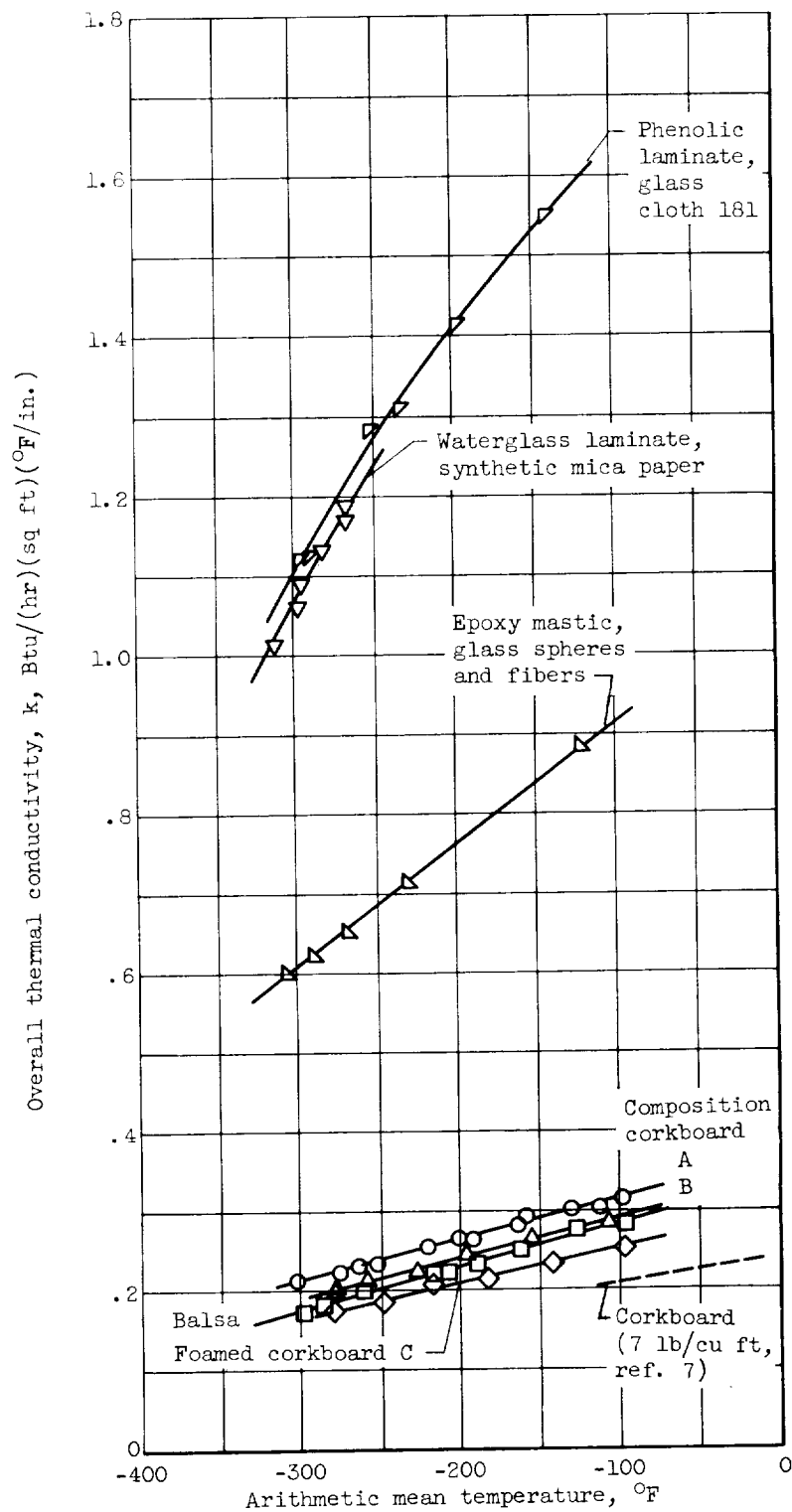


Figure 4. - Thermal-conductivity-meter results for self-supporting insulations (see table I).

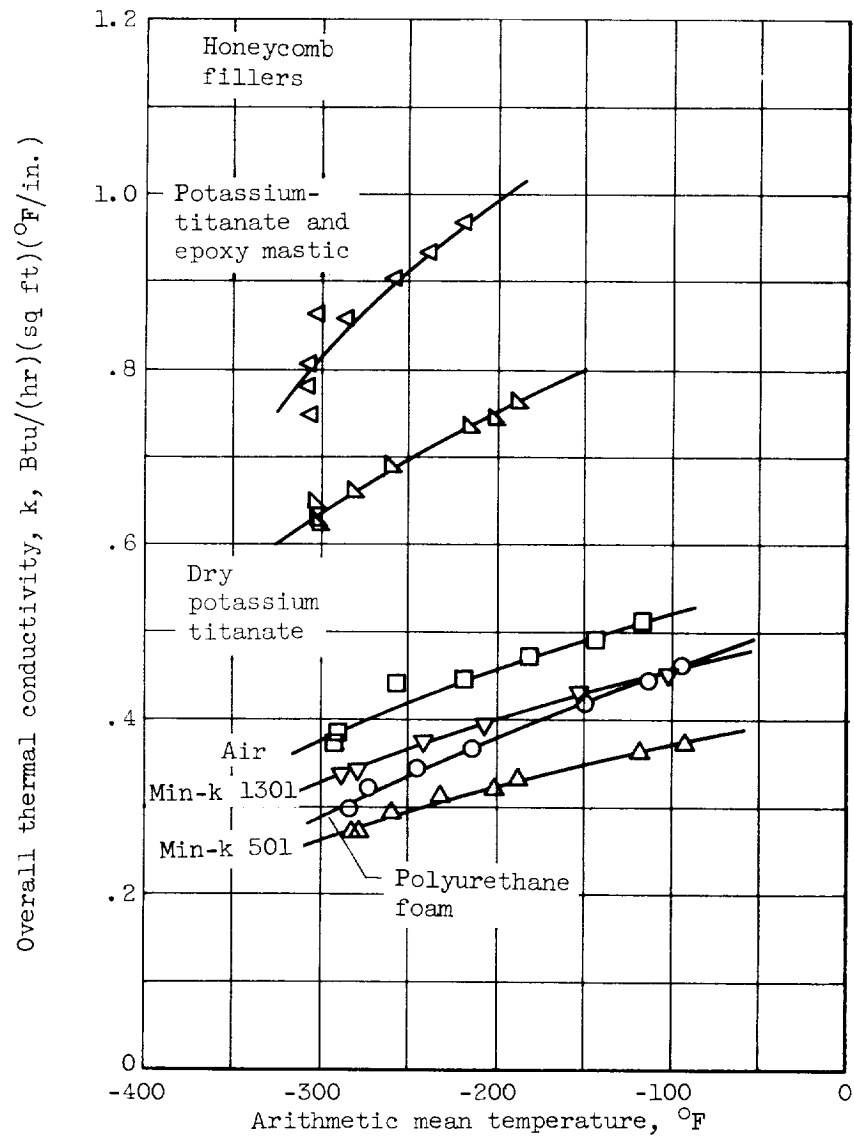
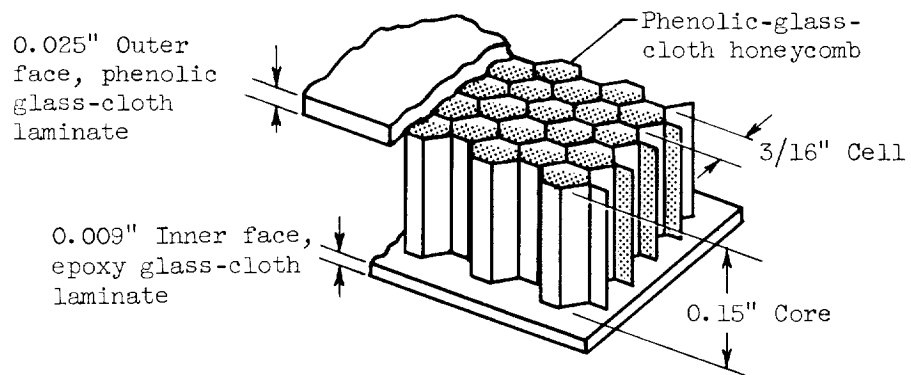


Figure 5. - Thermal conductivity-meter results for filled-honeycomb insulations.

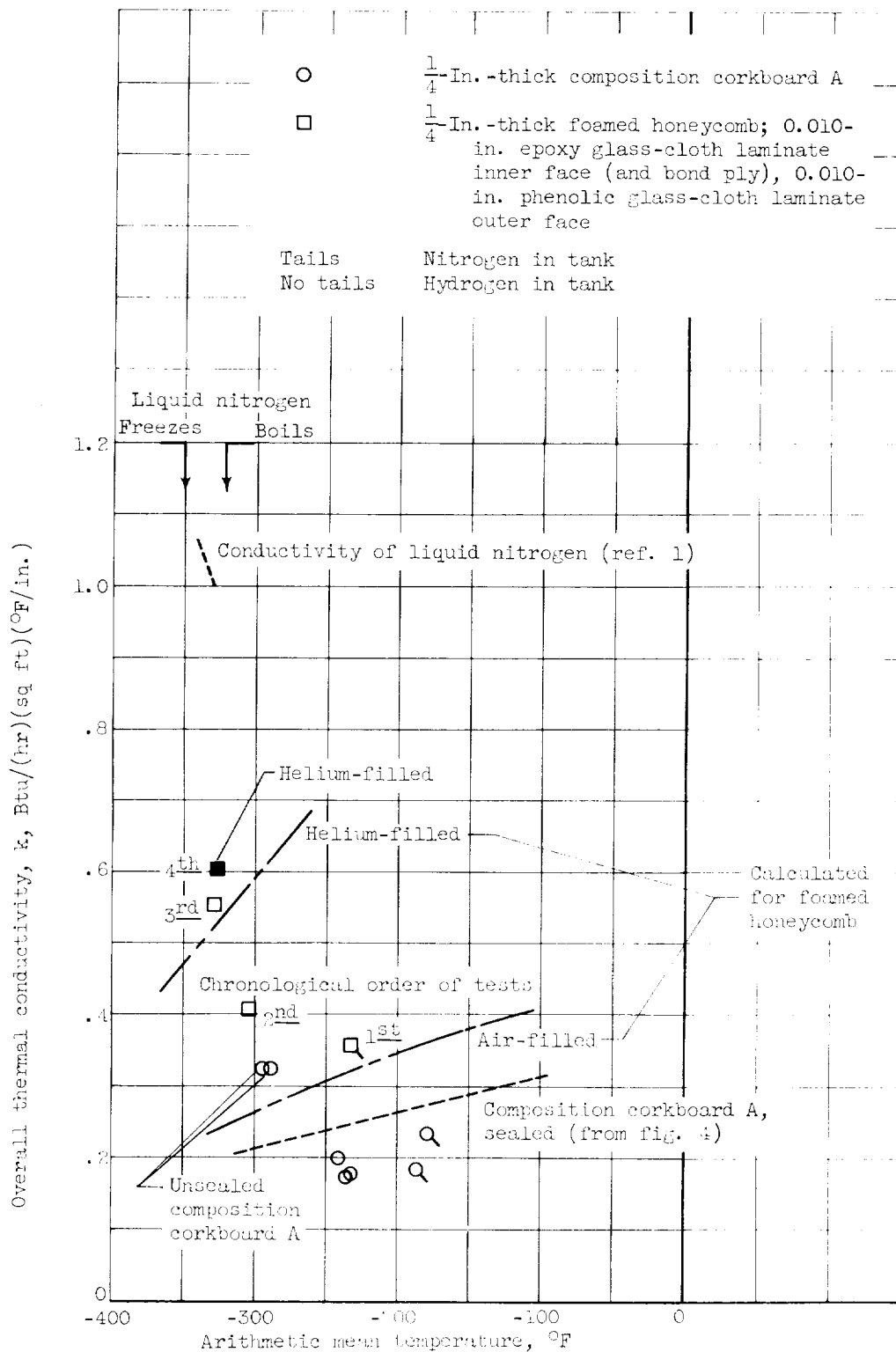






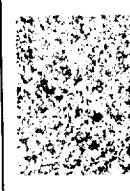
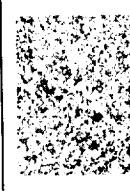

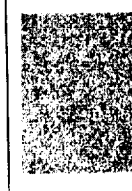
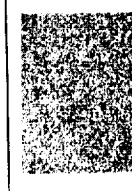

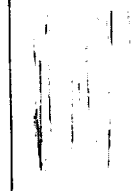
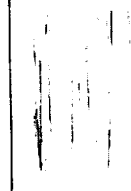

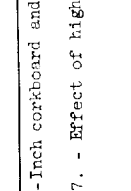


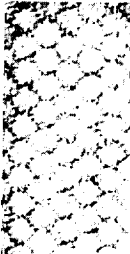



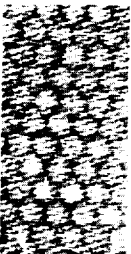
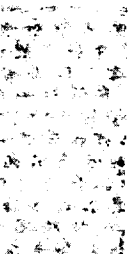




Figure 6. - Thermal conductivity of insulations from tank boiloff rates.

Specimen	Material and surface coat (table I)	Heating-cycle sequence*	Original condition	Appearance and approx. thickness (in.) after exposure to temp. (°F) of:	* Key to sequences of heating cycles
1	Composition corkboard A uncoated	S		 800° - 1/16"	Sequence of cycles, successive cycles, of sec Surface temp. in P 30 300, 400, 550, 670, 800 S 30 600, 700, 800 T 30 400, 550, 700, 850, 950, 1150, 1350 Z 50 Linear increase from 500° to 300° F in 40 sec; 10 sec at 900° F
2	Composition corkboard A epoxy-coated (q)	Z		 900° - 1/4"	
3	Composition corkboard A with phenolic varnish (P) and 0.001-in. Mylar (O)	T		 850° - 1/4"	 950° - 1/4"
4	Composition corkboard B with phenolic varnish (P) and 0.001-in. Mylar (O)	R		 400° - 1/4"	 550° - 1/4"
5	Foamed corkboard C with 0.001-in. Mylar (O)	R		 300° - 1/4"	 400° - 1/4"
6	Balsa with phenolic varnish (P) and 0.001-in. Mylar (O)	R		 300° - 1/4"	 550° - 1/4"

C-53900

(a) 1/4-Inch corkboard and balsa with various surface coatings (see table I).

Figure 7. - Effect of high-temperature, sonic-velocity gas flow on insulations.

Specimen	Facing material (table I)	Filler material (table I)	Heating- cycle sequence *	Original condition	After exposure to temp. (OF) of:
7	K (0.030-in. epoxy glass-cloth laminate)	J	Z		 300°
8	I (0.070-in. phenolic glass-cloth laminate)	J	Z		 300°
9	L (0.010-in. phenolic glass-cloth laminate with 0.001-in. Mylar)	G	T		 350°
10	M (0.012-in. phenolic- asbestos felt with 0.001-in. Mylar)	J	T		 350°
11	N (0.020-in. glass cloth impregnated with Silastic, plus 0.001-in. Mylar)	J	T		 550°

* See key on fig. 7(a).

(t) 1/4-inch-thick, 3/16-inch-core phenolic honeycomb with various facings and fillers.

Figure 7. - Concluded. Effect of high-temperature, sonic-velocity gas flow on insulations.

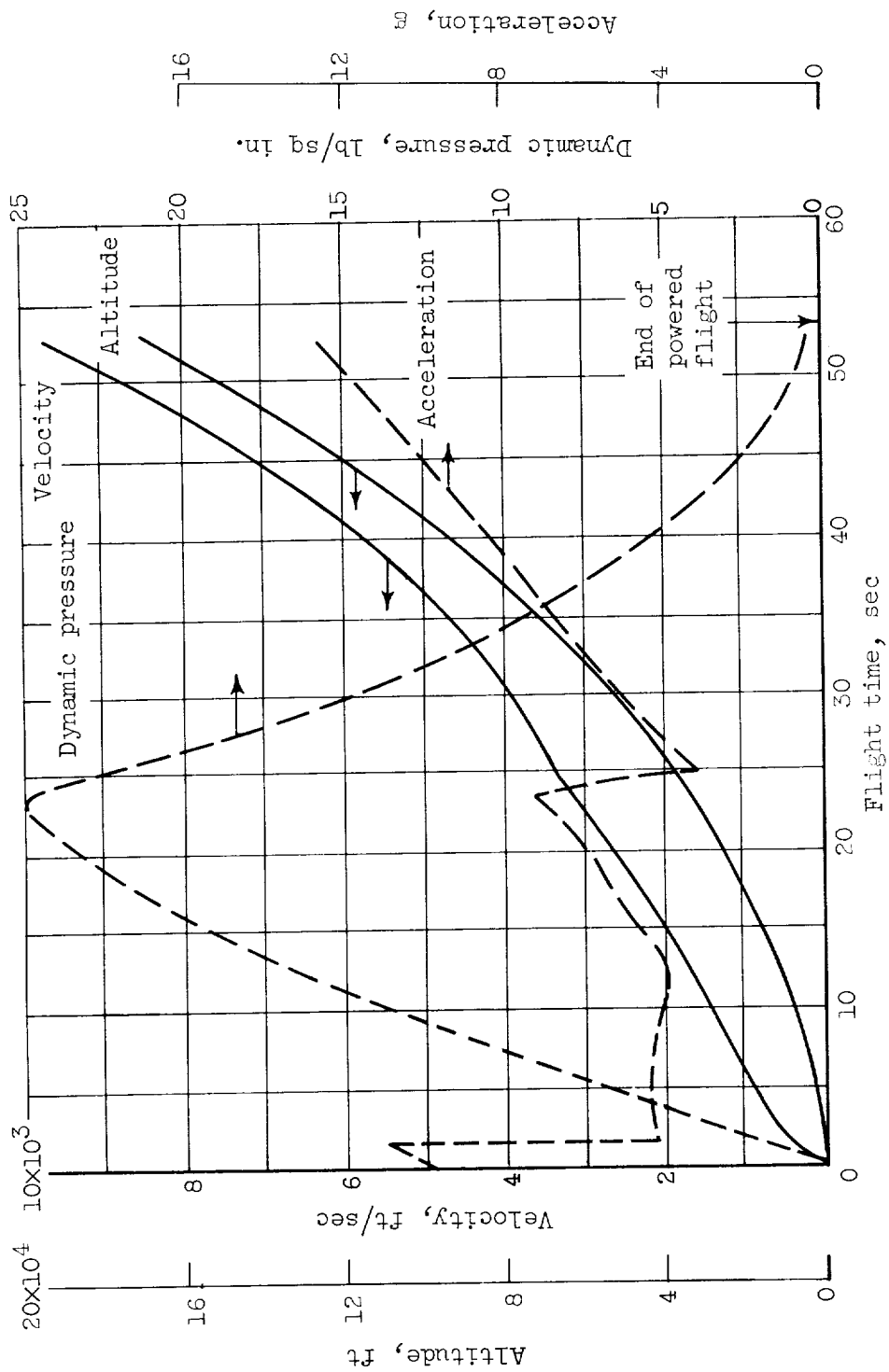


Figure 8. - Assumed flight plan for hydrogen-oxygen vehicle.

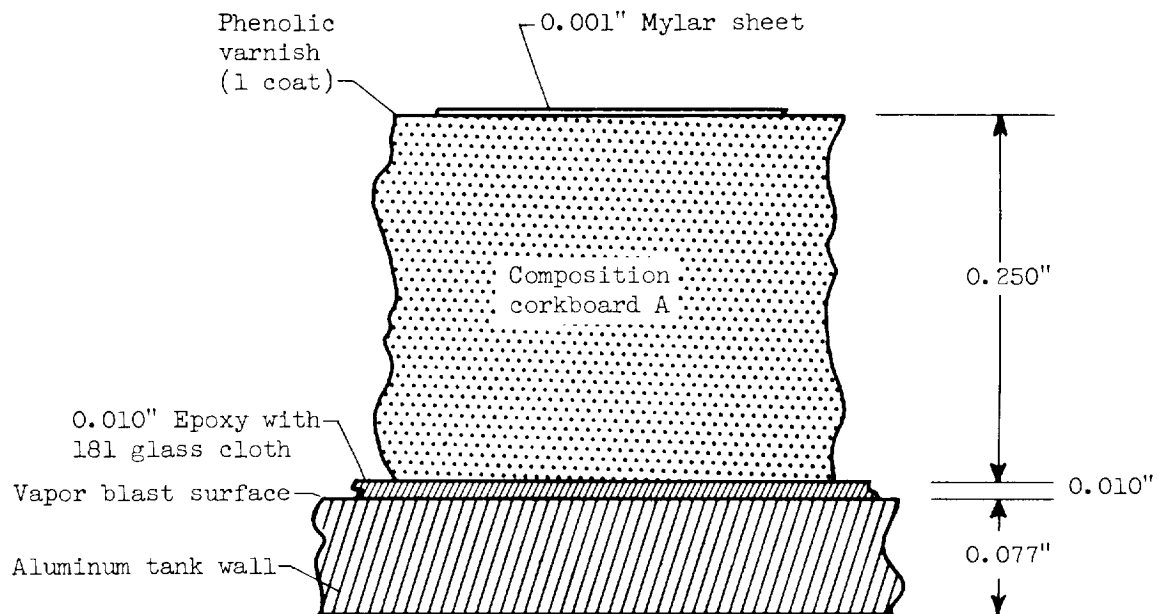


Figure 9. - Hydrogen-tank insulation design for assumed vehicle. Insulation weight, 0.53 pound per square foot; thermal conductivity, 0.26 Btu/(hr) (sq ft)(°F/in.) at mean temperature of -200° F (ref. fig. 4).

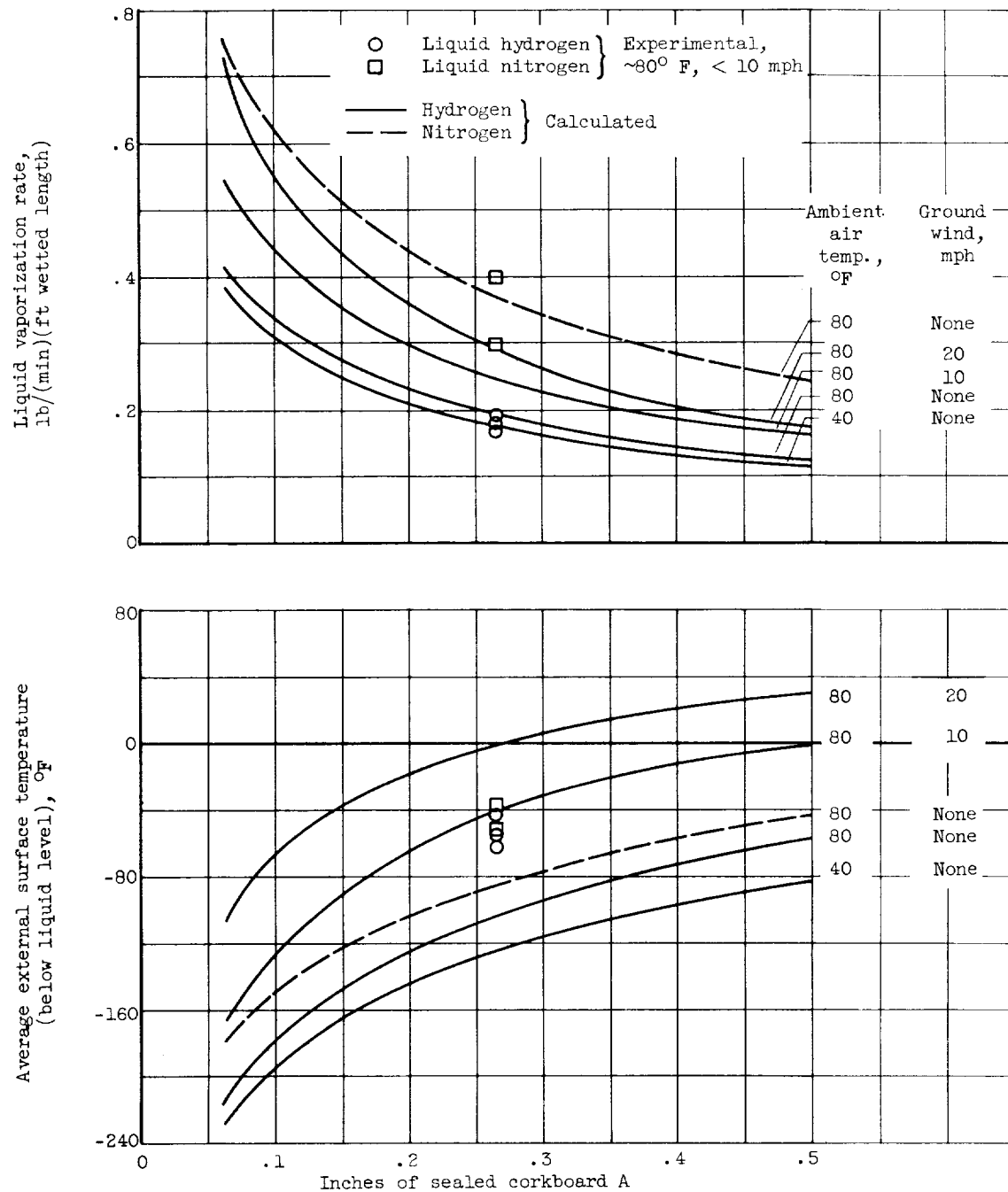


Figure 10. - Calculated ground performance of composition corkboard A insulation (including 0.010-in. bond ply) on a 32-inch-diameter tank (conductivity from fig. 4).

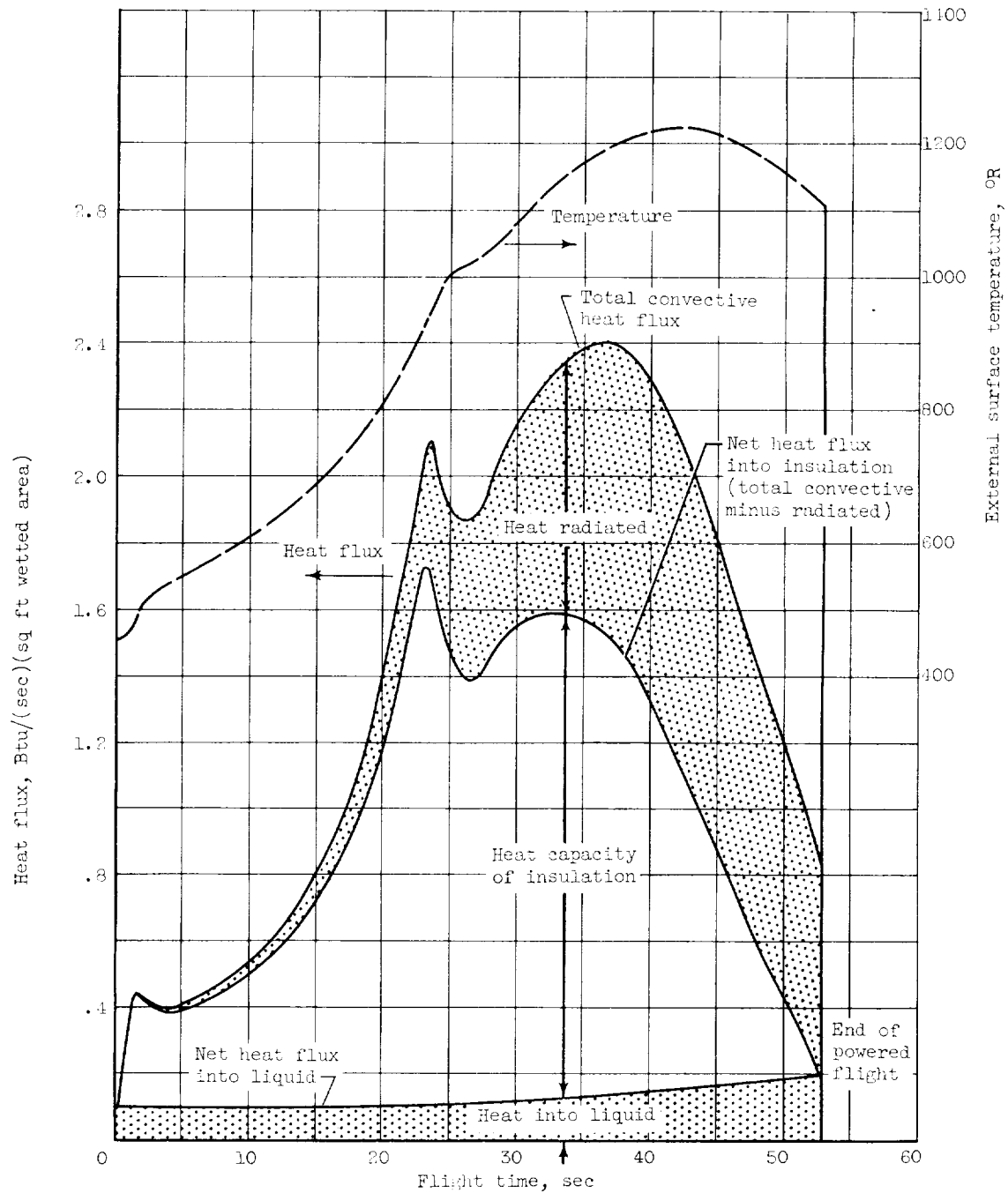


Figure 11. - Heat flux and external surface temperature of 1/4-inch-thick composition corkboard A bonded on hydrogen tank during assumed flight.

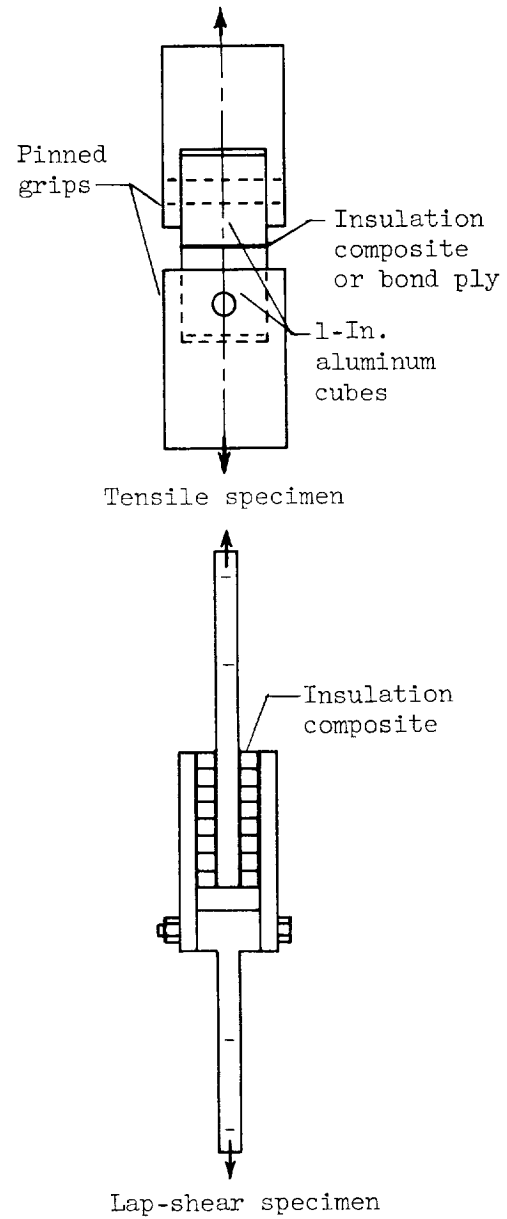
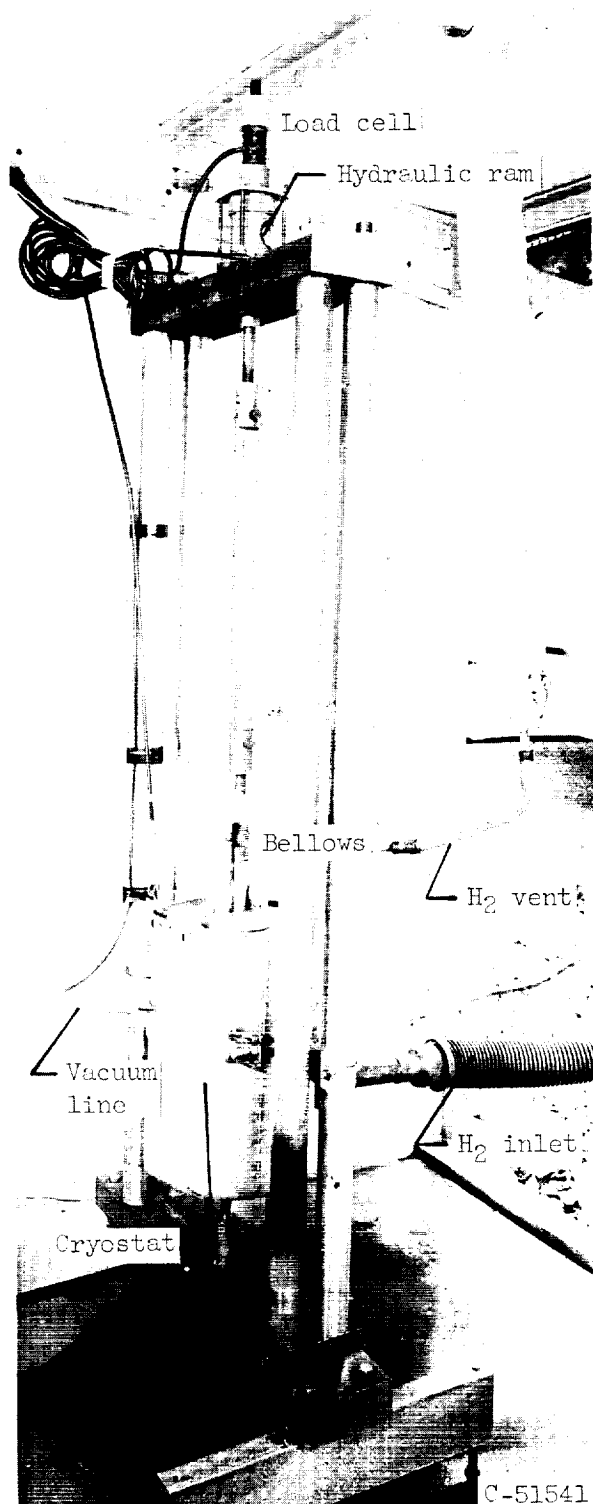


Figure 12. - Tensile machine with test chamber in place showing hydrogen supply and vent lines.

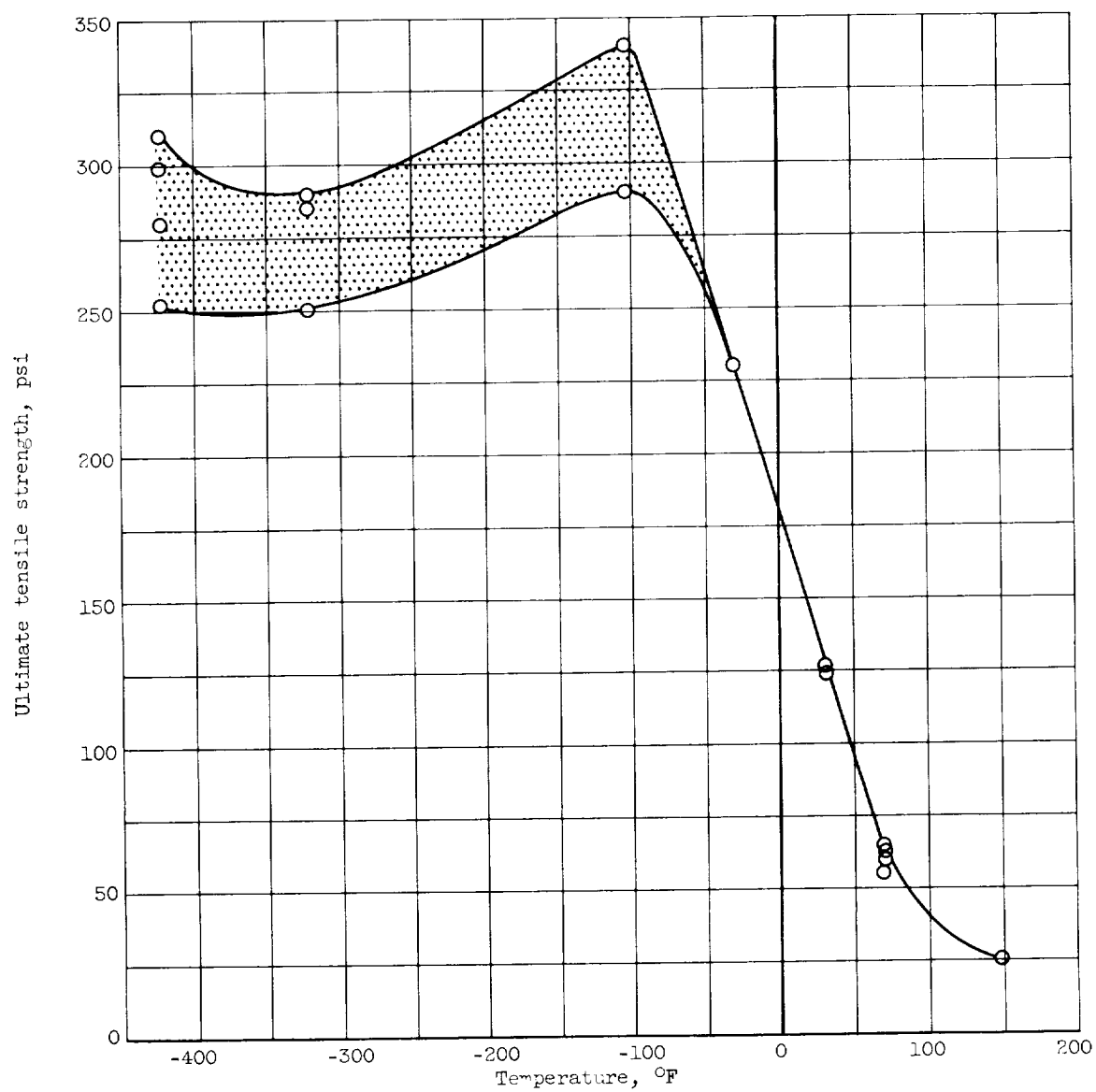


Figure 13. - Ultimate tensile strength of composition corkboard A as function of temperature.

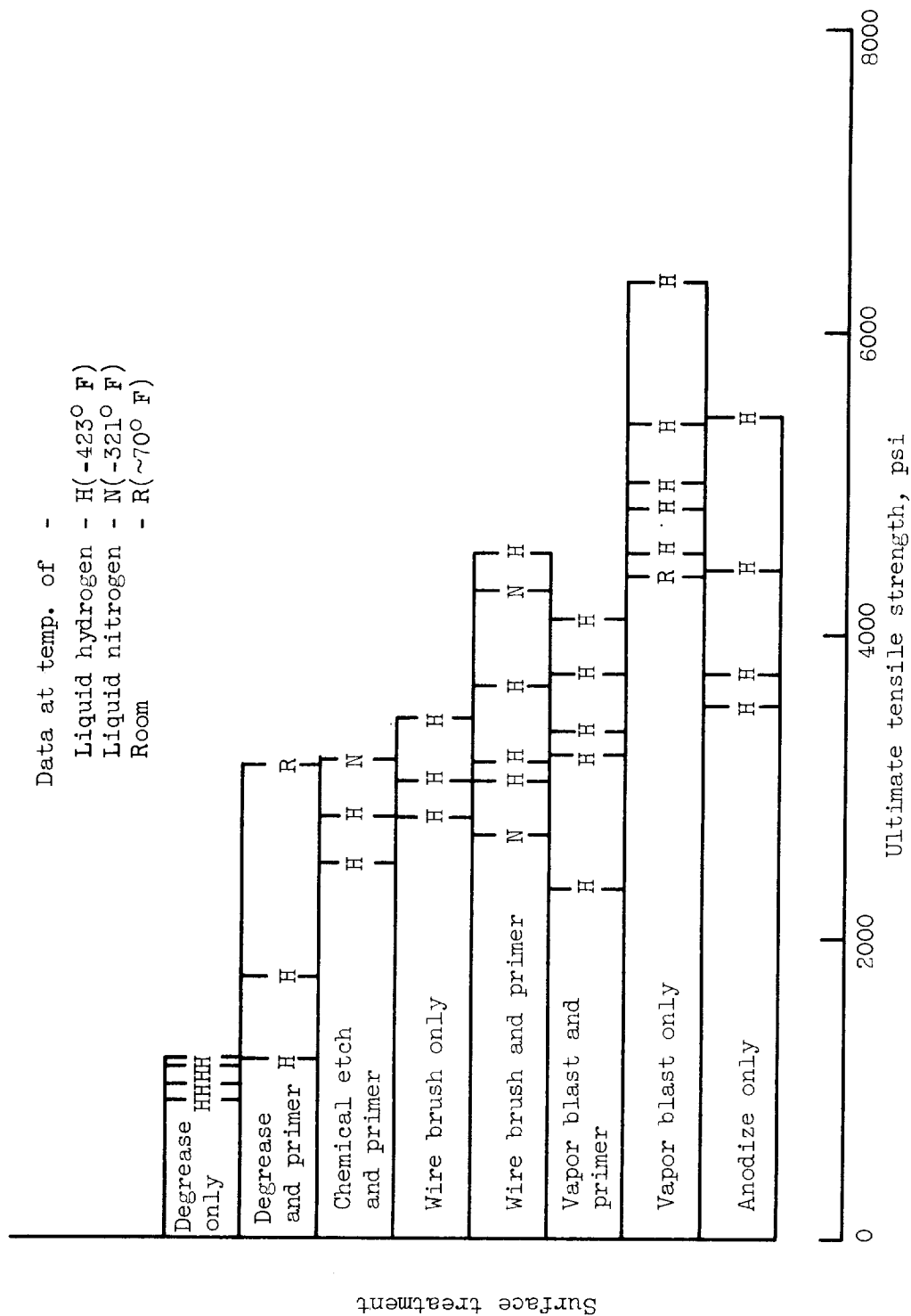


Figure 14. Bond strength of epoxy glass-cloth laminate (see table I) and aluminum.

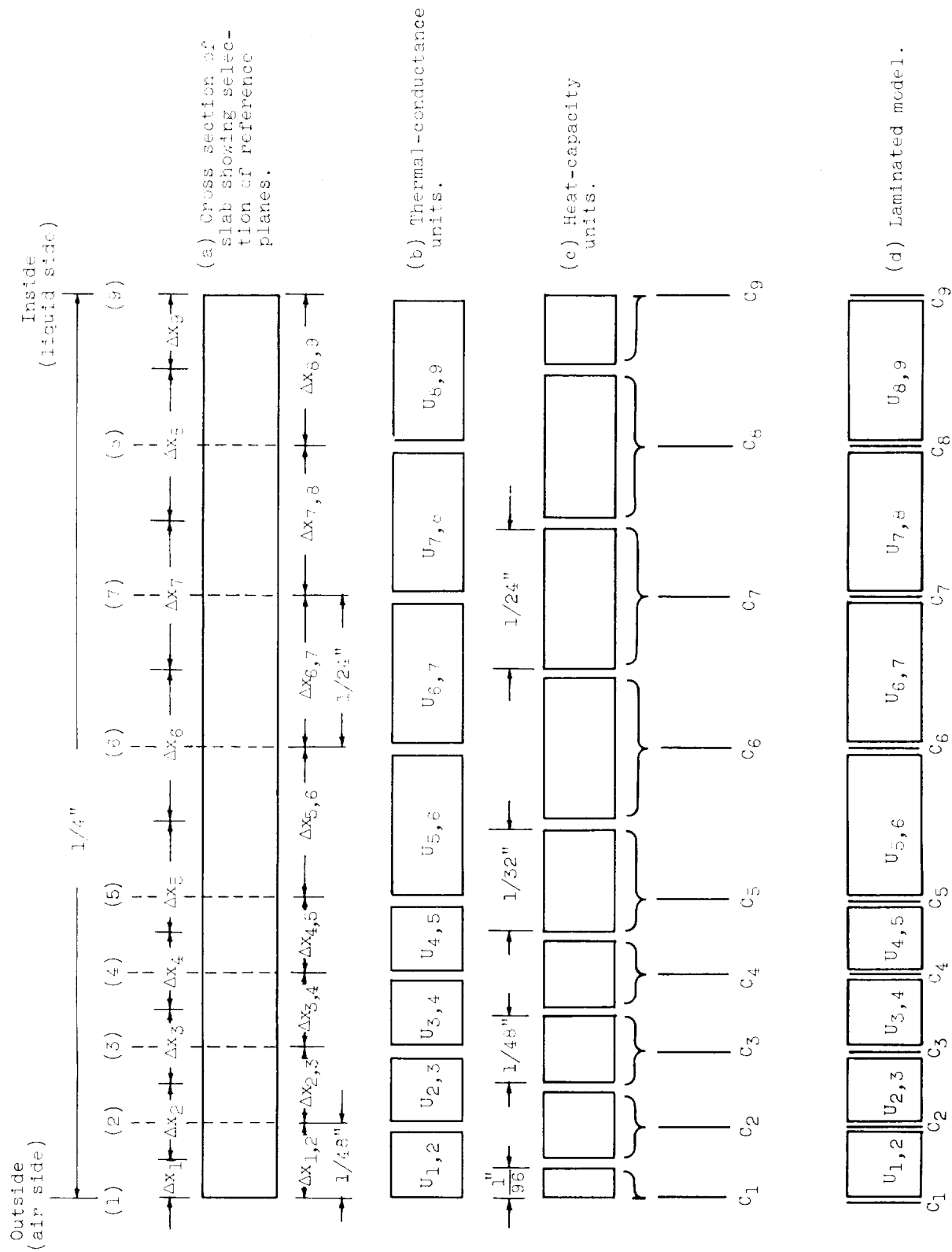


Figure 15. - Division of continuous slab into finite units of thermal conductance and heat capacity used in transient heating calculations.

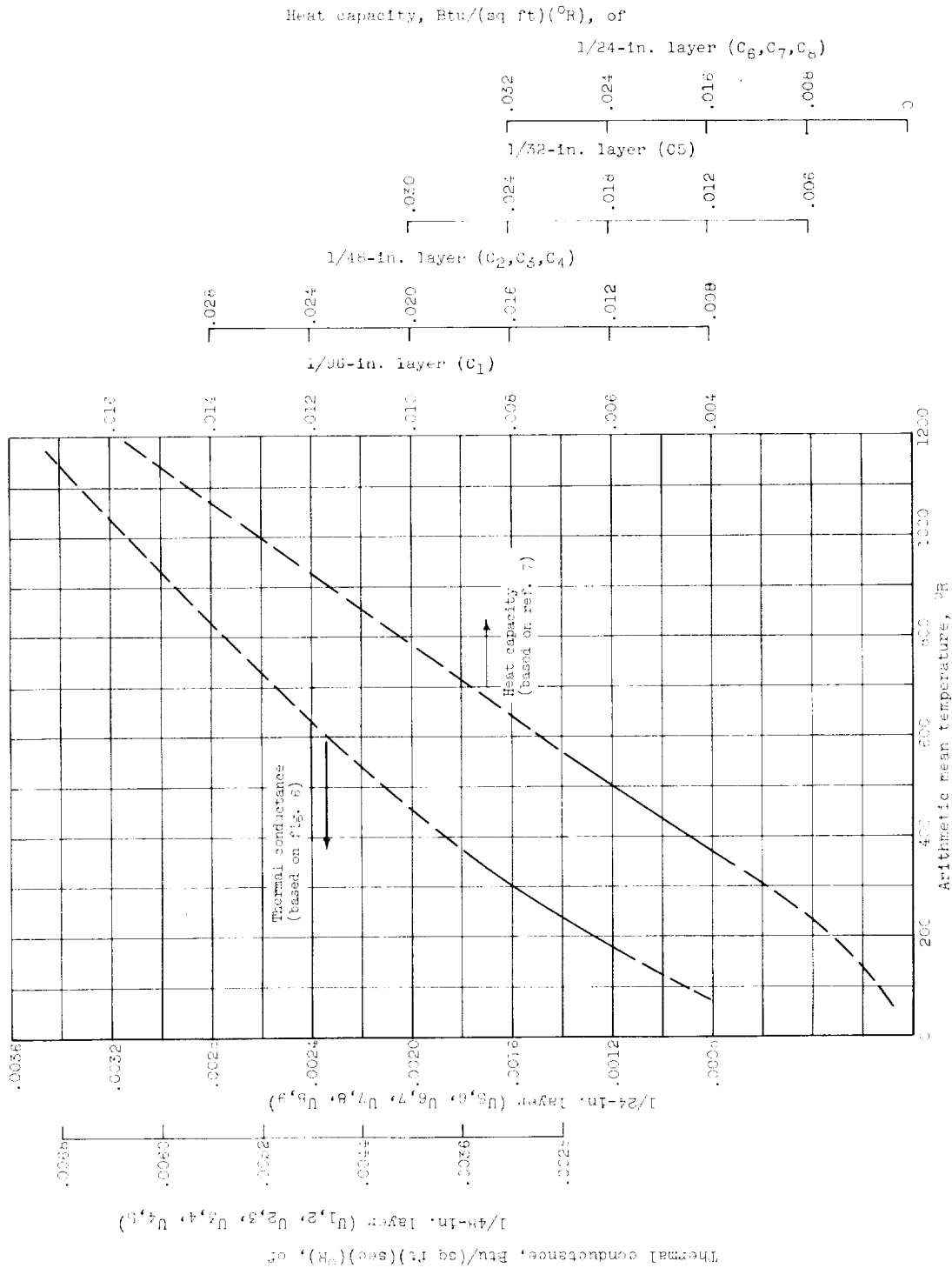


Figure 16. - Thermal conductance and heat capacity of composition corkboard A.

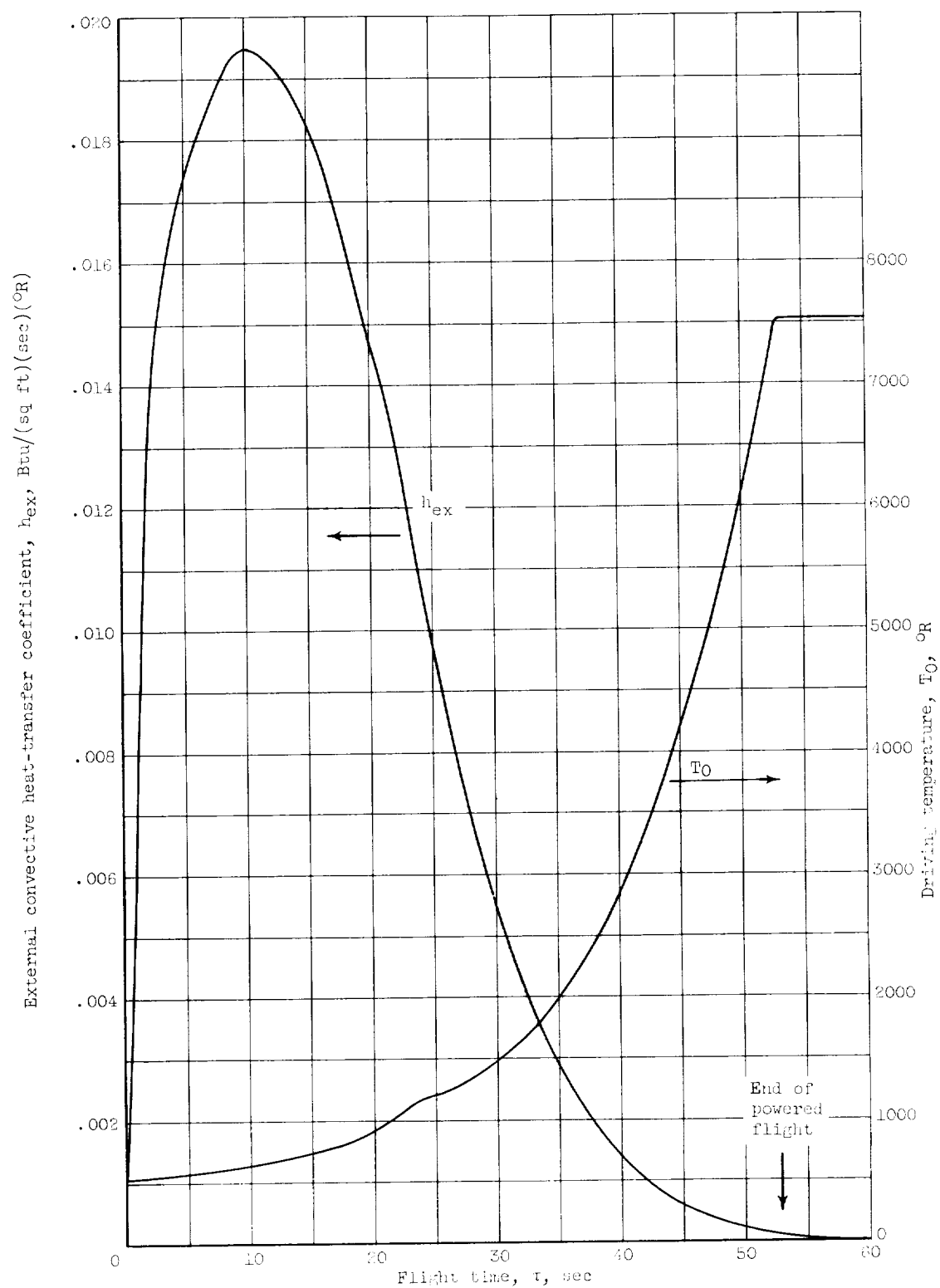


Figure 17. - External heat-transfer coefficient and driving temperature for assumed flight plan (Fig. 8 and ref. 16).

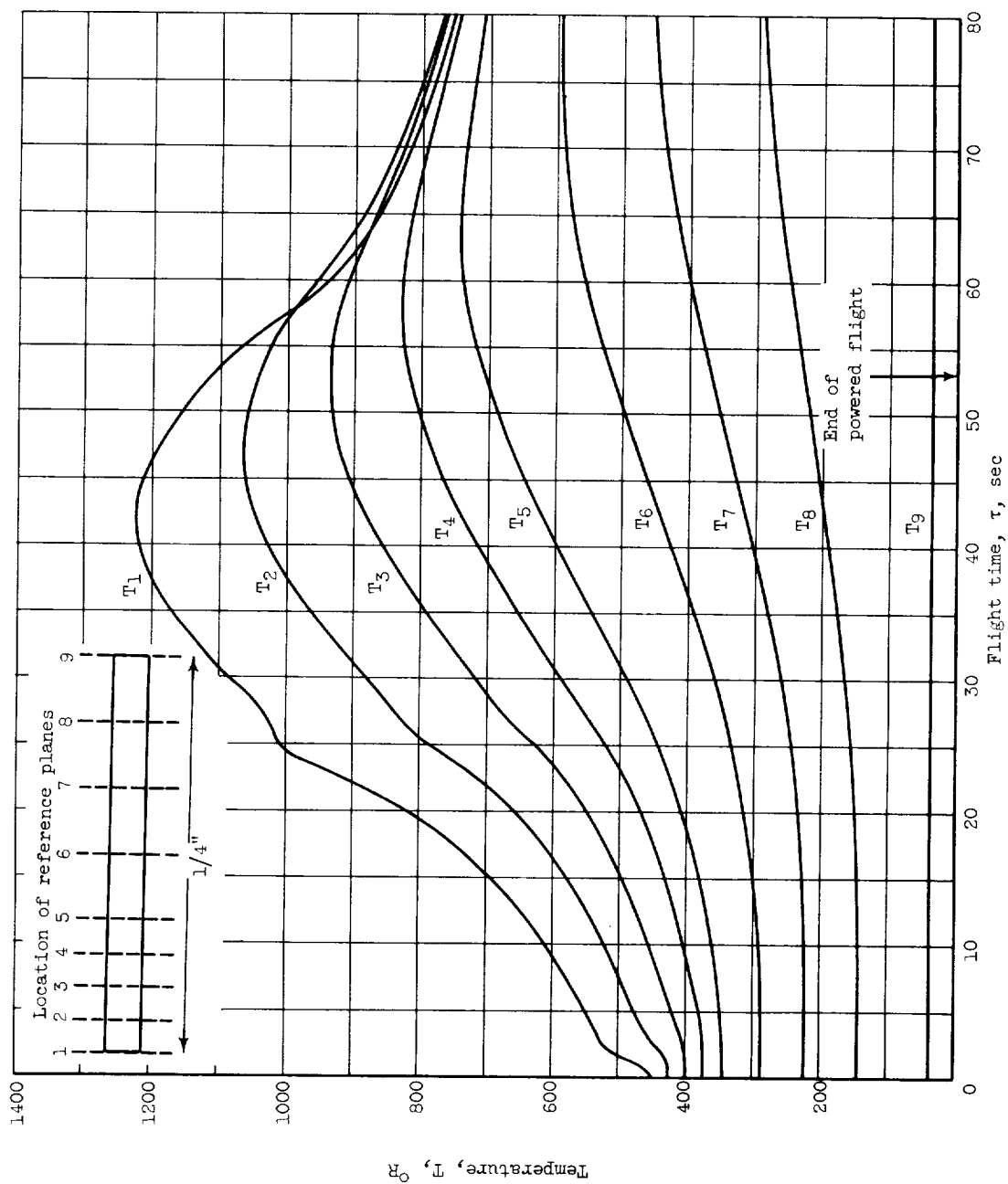


Figure 18. - Temperatures of reference planes within 1/4-inch-thick composition corkboard A during assumed flight plan plus 30-second coast.

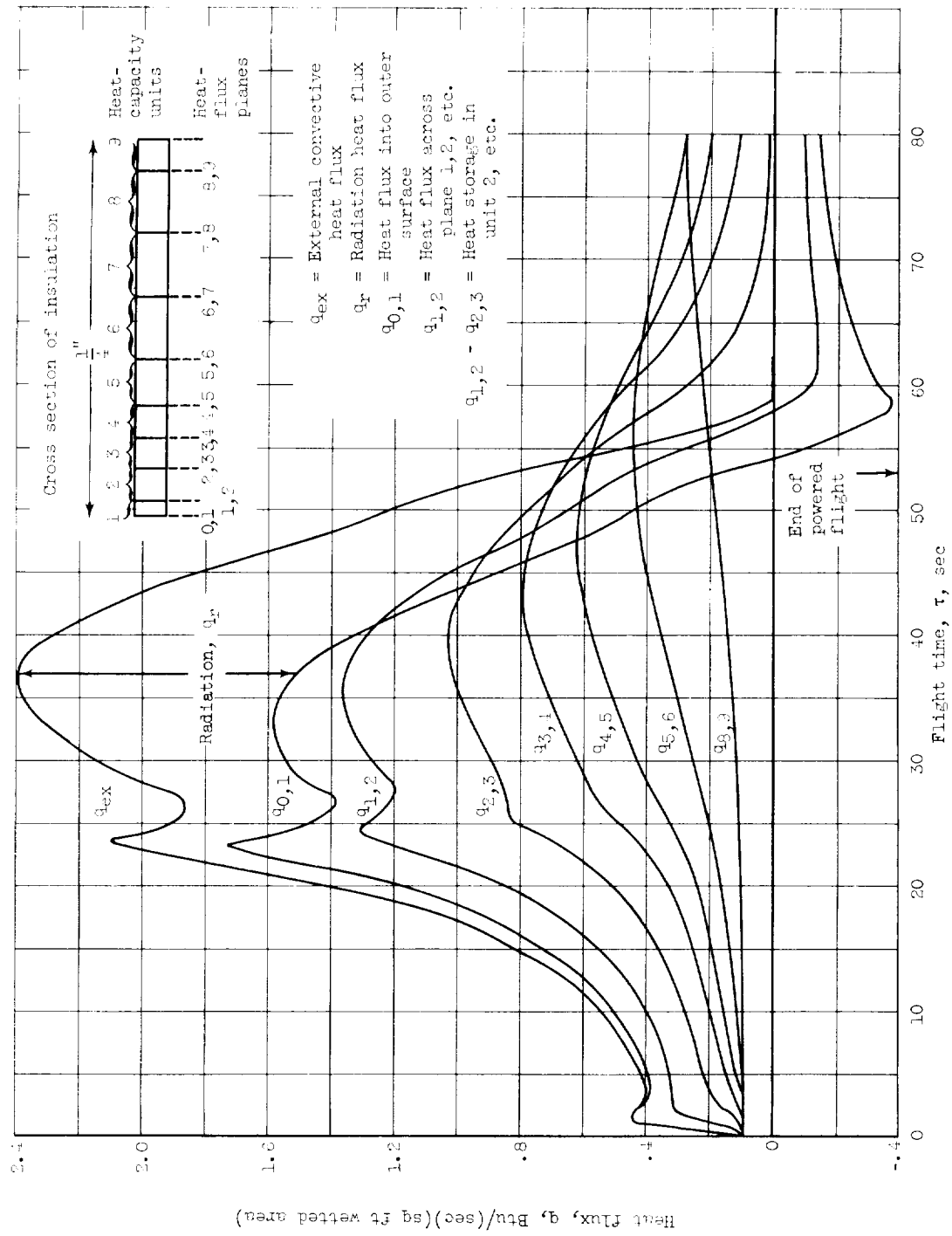


Figure 10. - Heat flux across reference layers of 1/4-inch-thick composition corkboard A during assumed flight plan plus 30-second coast.

<p>NASA TN D-476</p> <p>National Aeronautics and Space Administration.</p> <p>BONDED AND SEALED EXTERNAL INSULATIONS FOR LIQUID-HYDROGEN-FUELED ROCKET TANKS DURING ATMOSPHERIC FLIGHT. V. H. Gray, T. F. Gelder, R. P. Cochran, and J. H. Goodykoontz. APPENDIX B: STRENGTH OF INSULATIONS AND BOND TO ALUMINUM AT CRYOGENIC TEMPERATURES. Morgan P. Hanson. APPENDIX C: STEP METHOD OF APPROXIMATE NUMERICAL CALCULATION OF ONE-DIMENSIONAL TRANSIENT HEAT CONDUCTION WITH VARIABLE THERMAL PROPERTIES. William Lewis. October 1960. 51p. OTS price \$1.50. (NASA TECHNICAL NOTE D-476)</p> <p>Several currently available nonmetallic insulation materials that may be bonded onto liquid-hydrogen tanks and sealed against air penetration into the insulation have been investigated for application to rockets and spacecraft. Experimental data were obtained on the thermal conductivities of various materials in the cryogenic temperature range, as well as on the Copies obtainable from NASA, Washington (over)</p>	<p>I. Gray, Vernon H. II. Gelder, Thomas F. III. Cochran, Reeves P. IV. Goodykoontz, J. H. V. Hanson, Morgan P. VI. Lewis, William VII. NASA TN D-476</p> <p>(Initial NASA distribution: 25, Materials, engineering; 26, Materials, other; 28, Missiles and satellite carriers; 36, Propellants; 39, Propulsion systems, liquid-fuel; 52, Structures.)</p>	NASA
<p>NASA TN D-476</p> <p>National Aeronautics and Space Administration.</p> <p>BONDED AND SEALED EXTERNAL INSULATIONS FOR LIQUID-HYDROGEN-FUELED ROCKET TANKS DURING ATMOSPHERIC FLIGHT. V. H. Gray, T. F. Gelder, R. P. Cochran, and J. H. Goodykoontz. APPENDIX B: STRENGTH OF INSULATIONS AND BOND TO ALUMINUM AT CRYOGENIC TEMPERATURES. Morgan P. Hanson. APPENDIX C: STEP METHOD OF APPROXIMATE NUMERICAL CALCULATION OF ONE-DIMENSIONAL TRANSIENT HEAT CONDUCTION WITH VARIABLE THERMAL PROPERTIES. William Lewis. October 1960. 51p. OTS price \$1.50. (NASA TECHNICAL NOTE D-476)</p> <p>Several currently available nonmetallic insulation materials that may be bonded onto liquid-hydrogen tanks and sealed against air penetration into the insulation have been investigated for application to rockets and spacecraft. Experimental data were obtained on the thermal conductivities of various materials in the cryogenic temperature range, as well as on the Copies obtainable from NASA, Washington (over)</p>	<p>I. Gray, Vernon H. II. Gelder, Thomas F. III. Cochran, Reeves P. IV. Goodykoontz, J. H. V. Hanson, Morgan P. VI. Lewis, William VII. NASA TN D-476</p> <p>(Initial NASA distribution: 25, Materials, engineering; 26, Materials, other; 28, Missiles and satellite carriers; 36, Propellants; 39, Propulsion systems, liquid-fuel; 52, Structures.)</p>	NASA
<p>NASA TN D-476</p> <p>National Aeronautics and Space Administration.</p> <p>BONDED AND SEALED EXTERNAL INSULATIONS FOR LIQUID-HYDROGEN-FUELED ROCKET TANKS DURING ATMOSPHERIC FLIGHT. V. H. Gray, T. F. Gelder, R. P. Cochran, and J. H. Goodykoontz. APPENDIX B: STRENGTH OF INSULATIONS AND BOND TO ALUMINUM AT CRYOGENIC TEMPERATURES. Morgan P. Hanson. APPENDIX C: STEP METHOD OF APPROXIMATE NUMERICAL CALCULATION OF ONE-DIMENSIONAL TRANSIENT HEAT CONDUCTION WITH VARIABLE THERMAL PROPERTIES. William Lewis. October 1960. 51p. OTS price \$1.50. (NASA TECHNICAL NOTE D-476)</p> <p>Several currently available nonmetallic insulation materials that may be bonded onto liquid-hydrogen tanks and sealed against air penetration into the insulation have been investigated for application to rockets and spacecraft. Experimental data were obtained on the thermal conductivities of various materials in the cryogenic temperature range, as well as on the Copies obtainable from NASA, Washington (over)</p>	<p>I. Gray, Vernon H. II. Gelder, Thomas F. III. Cochran, Reeves P. IV. Goodykoontz, J. H. V. Hanson, Morgan P. VI. Lewis, William VII. NASA TN D-476</p> <p>(Initial NASA distribution: 25, Materials, engineering; 26, Materials, other; 28, Missiles and satellite carriers; 36, Propellants; 39, Propulsion systems, liquid-fuel; 52, Structures.)</p>	NASA
<p>NASA TN D-476</p> <p>National Aeronautics and Space Administration.</p> <p>BONDED AND SEALED EXTERNAL INSULATIONS FOR LIQUID-HYDROGEN-FUELED ROCKET TANKS DURING ATMOSPHERIC FLIGHT. V. H. Gray, T. F. Gelder, R. P. Cochran, and J. H. Goodykoontz. APPENDIX B: STRENGTH OF INSULATIONS AND BOND TO ALUMINUM AT CRYOGENIC TEMPERATURES. Morgan P. Hanson. APPENDIX C: STEP METHOD OF APPROXIMATE NUMERICAL CALCULATION OF ONE-DIMENSIONAL TRANSIENT HEAT CONDUCTION WITH VARIABLE THERMAL PROPERTIES. William Lewis. October 1960. 51p. OTS price \$1.50. (NASA TECHNICAL NOTE D-476)</p> <p>Several currently available nonmetallic insulation materials that may be bonded onto liquid-hydrogen tanks and sealed against air penetration into the insulation have been investigated for application to rockets and spacecraft. Experimental data were obtained on the thermal conductivities of various materials in the cryogenic temperature range, as well as on the Copies obtainable from NASA, Washington (over)</p>	<p>I. Gray, Vernon H. II. Gelder, Thomas F. III. Cochran, Reeves P. IV. Goodykoontz, J. H. V. Hanson, Morgan P. VI. Lewis, William VII. NASA TN D-476</p> <p>(Initial NASA distribution: 25, Materials, engineering; 26, Materials, other; 28, Missiles and satellite carriers; 36, Propellants; 39, Propulsion systems, liquid-fuel; 52, Structures.)</p>	NASA

<p>NASA TN D-476</p> <p>structural integrity and ablation characteristics of these materials at high temperatures occasioned by aerodynamic heating during atmospheric escape. Of the materials tested, commercial corkboard has the best overall properties for the specific requirements involved.</p> <p>Copies obtainable from NASA, Washington</p>	<p>NASA TN D-476</p> <p>structural integrity and ablation characteristics of these materials at high temperatures occasioned by aerodynamic heating during atmospheric escape. Of the materials tested, commercial corkboard has the best overall properties for the specific requirements involved.</p> <p>Copies obtainable from NASA, Washington</p>	<p>NASA</p>
<p>NASA TN D-476</p> <p>structural integrity and ablation characteristics of these materials at high temperatures occasioned by aerodynamic heating during atmospheric escape. Of the materials tested, commercial corkboard has the best overall properties for the specific requirements involved.</p> <p>Copies obtainable from NASA, Washington</p>	<p>NASA TN D-476</p> <p>structural integrity and ablation characteristics of these materials at high temperatures occasioned by aerodynamic heating during atmospheric escape. Of the materials tested, commercial corkboard has the best overall properties for the specific requirements involved.</p> <p>Copies obtainable from NASA, Washington</p>	<p>NASA</p>